RIS Assisted UAV for Weather-Dependent Satellite Terrestrial Integrated Network With Hybrid FSO/RF Systems

Xin Li, Yongjun Li, Xinkang Song, Long Shao, and Hai Li

***Abstract*—In this paper, we investigate the performance of hybrid free-space optical (FSO) and radio frequency (RF) relay systems in satellite terrestrial integrated network where the effect of weather conditions is taking into consideration. Specifically, we design three different relay schemes in different weather conditions based on high-altitude platform station (HAPS) and reconfigurable intelligent surface (RIS) assisted unmanned aerial vehicle (UAV). The RF link is modeled by shadowed Rician model while the FSO link is assumed to follow the Gamma-Gamma distribution in the presence of path loss, pointing errors and angle-of-arrival (AOA) fluctuations where it operates under either intensity modulation with direct detection (IM/DD) or heterodyne detection (HD). The performance of our proposed scheme is evaluated in terms of outage probability, average bit-error rate (BER) and ergodic capacity in the form of bivariate Fox's H function and bivariate Meijer's G function. Moreover, asymptotic results and diversity order for the outage and average BER at high signal-to-noise ratio (SNR) regime are also obtained to get more insights. Finally, numerical results and comparison scheme are provided to verify the accuracy and superiority of our scheme.**

***Index Terms*—Average bit-error rate (BER), ergodic capacity, hybrid radio frequency (RF)/free-space optical (FSO), outage probability, reconfigurable intelligent surface (RIS), relay link, satellite terrestrial integrated network.**

I. Introduction

A. Background

RECENTLY, with the explosive growth of people's demand for seamless reliable and high data rate services at anytime and anywhere on the earth, the traditional terrestrial network has been unable to meet this demand [1], [2]. Fortunately, due to the development of satellite communication technology, the popularity of high-altitude platform station (HAPS) and maturity of unmanned aerial vehicles (UAV) technology, the satellite terrestrial integrated network along with aerial network is a promising development trend for future sixth-generation (6G) wireless communications [3], [4]. More specifically, the HAPS or UAV can be used as a relay node to forward signals from satellite to different ground stations (GS) [5].

Free space optical (FSO) communication has attracted great attention due to its advantages over radio frequency (RF) communication, such as very high bandwidth, heavily secured links, robustness to electromagnetic interference, and ease of deployment [6], [7], [8]. In addition, the combination of FSO communication and satellite technology can achieve ubiquitous coverage and high transmission capacity which can meet the future requirements [9], [10]. However, FSO communication requires perfect line-of-sight (LOS) connectivity due to its narrow transmit bandwidth. Furthermore, the fading caused by atmospheric turbulence and weather conditions such as cloud, fog and snow will have an enormous impact on FSO communication [11], [12], [13], [14]. In comparison, the RF communication is only sensitive to rainy weather, and these different kinds of weather rarely occur at the same time. Therefore, FSO link and RF link can serve as complementary link to reduce the impact of weather conditions.

Relay technology is another alternative means to reduce the impact of weather conditions on FSO communication [15], [16]. Due to the advantages of flexible deployment, easy maintenance, less costs and environmental friendliness, HAPS is widely used in astronomy, disaster monitoring, and emergency communication [17], [18]. Therefore, HAPS can be used as the relay node between satellite and GS to further improve the performance of FSO communication. The HAPS can operate at the altitudes of 17–32 km above sea level and the satellite-to-GS downlink can be split into two parts: 1) satellite-to-HAPS link and 2) HAPS-to-GS link. Considering the actual atmospheric conditions, the HAPS-to-GS FSO link will be more affected by weather conditions. Hence, it is necessary to use this link together with the RF link or perform spatial diversity. The reconfigurable intelligent surface (RIS) assisted UAV is a better choice to performing spatial diversity [19], [20].

B. Related Works

Hybrid FSO/RF communication and relay communication have been fully studied in the terrestrial network [21], [22]. The physical layer security (PLS) performance of hybrid FSO/RF communication system was studied in [21], optimal power allocation optimization and diversity technology were also used

Manuscript received 29 May 2023; revised 4 September 2023; accepted 10 September 2023. Date of publication 12 September 2023; date of current version 26 September 2023. This work was supported by the Natural Science Foundation of Shaanxi Province under Grant/Award 2023-JC-QN-0084. *(Corresponding author: Xin Li.)*

The authors are with the Information and Navigation College, Air Force Engineering University, Xi'an 710077, China (e-mail: 1300358390@qq.com; tz_228@163.com; songxinkang_fly@163.com; anthonyalone@outlook.com; hailee1aa@gmail.com).

Digital Object Identifier 10.1109/JPHOT.2023.3314664

to further improve system performance. Considering the multiuser terrestrial amplify-and-forward (AF) relay system with FSO/RF links, the author in [22] presented a detail analysis of the system outage performance. Recently, the research of the hybrid FSO/RF system was also extended to the satellite terrestrial integrated network [23], [24]. In [23], the performance of satellite terrestrial hybrid FSO/RF link with high throughput FSO feeder link was studied, and the nonlinearity of satellite power amplifier was also taken into account. The author in [24] discussed the impact of rain attenuation on the outage performance and ergodic capacity of hybrid FSO/RF links. The influence of solar scintillation on the performance of hybrid FSO/RF link was studied in [25], [26], and some intractable challenges and improvement methods were also addressed.

However, in some cases such as clouds obstruction, the LOS link between HAPS and GS may not exist, an alternative method is to deploy an UAV as a relay node to forward signal to the GS. The channel modeling and parameter optimization about UAV were sufficiently studied in [27], [28]. Considering the multiuser scheduling for asymmetric FSO/RF links in satellite-UAV-terrestrial network, the author in [29] proposed a fairness resource scheduling method base on Jain's fairness index (JFI). In order to improve the outage performance of the satellite-aerial-terrestrial network with mixed FSO/RF channels, a robust beamforming scheme was proposed in [30]. A rate adaptation scheme based on satellite-HAPS-UAV-terrestrial network was proposed in [31], by reducing frequently switching between FSO and RF, the system outage performance and spectrum efficiency were improved compared with fixed rate design. Recently, RIS has also been applied to FSO/RF relay communication. In [32], the author proposed a dual-hop RIS based FSO/RF communication system, where the RIS was utilized to improve the coverage and system performance. Taking satellite-UAV-terrestrial network into consideration, a RIS-assisted hybrid FSO/RF link with pointing errors and phase shift errors was analyzed in [33], diversity order and coding gain were also obtained to get more insights. In [34], a RIS assisted hybrid FSO/RF satellite-aerial-ground network was proposed where RIS was used to reflect the signals from the HAP, but a closed-form solution and asymptotic analysis were not obtained in this paper.

C. Motivation and Contribution

For the case of satellite terrestrial integrated network, most of existing studies have focused on collaborative switching and relay transmission of FSO link and RF link. However, due to the effect of complex weather conditions, FSO link and RF link may face performance degradation or even unavailability in some case. Moreover, even in clear weather condition, FSO link may face the situation where it is unavailable due to cloud block. It is very essential to study the cooperative transmission strategy of FSO link and RF link under complex weather conditions. Few works have investigated from the weather conditions perspective and to the best of the authors' knowledge, only research works [35] and [36] have made preliminary research on the impact of weather conditions on FSO/RF system. In [35], considering the effect of weather conditions, a hybrid RF/FSO transmission strategy for satellite communication system was proposed for improving power efficiency. In our previous work [36], the performance of weather-dependent satellite terrestrial integrated network with rate adaptation hybrid FSO/RF link was analyzed. However, both of the above works didn't take the impact of relay links into consideration which are of great importance for increasing the duration of each session and further improving the link performance. Motivated by this, the main contributions of our proposed work are summarized as follows:

- We give a detail description of our proposed weather-dependent hybrid FSO/RF systems and the channel model for three different relay schemes, which includes: the dual-hop FSO relay link based on HAPS, the three-hop FSO relay link based on HAPS and RIS assisted UAV, and the dual-hop FSO/RF relay link based on HAPS. Moreover, a description of the weather-dependent link selection scheme is also presented.
- We consider the RIS assisted UAV as a relay node to achieve spatial diversity of FSO link, and the impact of (angle-of-arrival) AOA fluctuation on system performance is also analyzed.
- Based on the expressions of end-to-end signal-to-noise ratio (SNR), we derive the information-theoretic metrics including outage probability, average bit-error rate (BER) of different modulation schemes, and ergodic capacity, which are in terms of bivariate Fox's H function and bivariate Meijer's G function. Furthermore, asymptotic results and diversity order for outage probability and average BER at high SNR regime are also obtained to get more insights.
- The system performance can be significantly improved by reducing turbulence level and increasing pointing error parameters. Moreover, the system outage probability and average BER will tend to a saturation in some case. Besides, the diversity orders of outage probability and average BER are determined by the smallest values of turbulence parameters and pointing errors.
- Our proposed scheme owns significant performance advantages compared to the existing schemes which can be apply to the satellite terrestrial integrated network. In addition, due to the AOA fluctuation of UAV, there will exist a lower limit in link outage probability and average BER.

The remainder of this paper is organized as follows. In Section II, the system and channel models along with link switching scheme are outlined. We derive the closed-form expressions of outage probability, average BER and the ergodic capacity in Section III and the asymptotic results at high SNR regime are presented in Section IV. Section V presents the numerical and simulation results to illustrate the system performance. Finally, concluding remarks are drawn in Section VI.

II. System and Channel Models

In this paper, we consider a downlink satellite communication scenario, where the LEO satellite aims to communicate with GS through a relay link. The reason why we adopt HAPS as relay node is to counteract the impact of weather effects and further improve the system performance. As shown in Fig. 1, the FSO

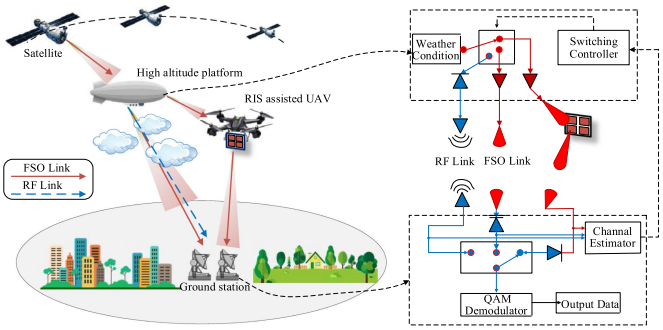

Fig. 1. Architecture of weather-dependent satellite terrestrial integrated network with hybrid FSO/RF systems.

link is adopted between satellite and HAPS, while the hybrid FSO/RF links are used between HAPS and GS. The system has four working modes: respectively named mode-1, mode-2, mode-3 and mode-4. For mode 1, we consider clear weather condition without cloud where FSO link is in good quality. For mode 2, we consider rainy weather where RF link is in worse condition. For mode 1 and mode 2, the LOS FSO link between HAPS and GS is available, and AF relay under a fixed gain Q is adopted. For mode 3, a RIS assisted UAV is deployed to forward signal to the GS under a fixed gain Q when the LOS FSO link between HAPS and GS becomes unavailable, which is mainly due to clouds obstruction. For mode 4, the RF link is used to transmit the signal to GS when the FSO link is unavailable due to foggy weather.

A. Satellite-HAPS-GS Signal Model

At the satellite, the data modulated by quadrature amplitude modulation (QAM) can be expressed as

$$s_n(t) = A_{nI}(t)g(t)\cos(2\pi f_c t) - A_{nQ}(t)g(t)\sin(2\pi f_c t) \tag{1}$$

Where f_c is the carrier frequency, $g(t)$ is the pulse shaping function, A_{nI} and A_{nQ} are the in-phase and orthogonal component of the amplitude [34], respectively. Then, the transmitted optical signal modulated by QAM signal is given as

$$s(t) = P_t\left[1 + m_0 s_n(t)\right] \tag{2}$$

Where P_t is the transmitted power at satellite, m_0 is the modulation index ($0 < m_0 < 1$) which ensures that the laser avoids over-modulation induced clipping. At the HAPS, the received optical signal is forwarded to GS under different relay modes. For mode 1, the optical signal is directly forwarded to GS, so the received SNR γ_{SH}^f and output signal $y_{Hf}(t)$ at HAPS can be expressed as

$$\gamma_{SH}^f = \frac{\left(h_{SH}^f m_0 P_t\right)^2}{\sigma_{n_{SH}^f}^2} = \bar{\gamma}_{SH}^f \left(h_{SH}^f\right)^2 \tag{3}$$

$$y_{Hf}(t) = G_{FSO}\left[h_{SH}^f s(t) + n_{SH}^f\right] \tag{4}$$

Where h_{SH}^f is the channel coefficient of the satellite-to-HAPS FSO link, $\bar{\gamma}_{SH}^f = \frac{m_0^2 P_t^2}{\sigma_{n_{SH}^f}^2}$ is the average SNR, G_{FSO} is the amplification factor limited by the maximum transmit power of HAPS, n_{SH}^f is the additive white Gaussian noise (AWGN) with variance $\sigma_{n_{SH}^f}^2$. The received signal $y_{Gf}(t)$ and SNR γ_{HG}^f at GS by mode 1 is shown as

$$y_{Gf}(t) = h_{HG}^f \eta G_{FSO}\left[h_{SH}^f s(t) + n_{SH}^f\right] + n_{HG}^f \tag{5}$$

$$\gamma_{HG}^f = \frac{\left(\eta h_{HG}^f G_{FSO} h_{SH}^f m_0 P_t\right)^2}{\left(\eta h_{HG}^f G_{FSO}\sigma_{n_{SH}^f}\right)^2 + \sigma_{n_{HG}^f}^2} \tag{6}$$

Where h_{HG}^f is the channel coefficient of the HAPS-to-GS FSO link, η is the optical-to-electrical conversion coefficient, n_{HG}^f is the AWGN with variance $\sigma_{n_{HG}^f}^2$. For mode 2, we consider rainy weather and the optical signal is also directly forwarded to GS. Therefore, the working mechanism of mode 1 and mode 2 is the same which is HAPS based FSO/FSO relay link while with different channel parameters, so we don't provide any additional introduction for mode 2 here.

For mode 3, the optical signal is firstly forwarded to UAV and then reflected to GS by RIS, so the received signal $y_{Gu}(t)$ and SNR γ_{HG}^u at GS can be expressed as

$$y_{Gu}(t) = h_{HG}^u \eta G_{FSO}\left[h_{SH}^f s(t) + n_{SH}^u\right] + n_{HG}^u \tag{7}$$

$$\gamma_{HG}^u = \frac{\left(\eta h_{HG}^u G_{FSO} h_{SH}^f m_0 P_t\right)^2}{\left(\eta h_{HG}^u G_{FSO}\sigma_{n_{SH}^f}\right)^2 + \sigma_{n_{HG}^u}^2} \tag{8}$$

Where h_{HG}^u is the channel coefficient of the HAPS-to-GS RIS assisted FSO link, n_{HG}^u is the AWGN with variance $\sigma_{n_{HG}^u}^2$. For mode 4, the optical signal is first converted into an RF signal by a photodiode and then forwarded to GS, so the received signal $y_{Gr}(t)$ and SNR γ_{HG}^r at GS can be expressed as

$$y_{Gr}(t) = h_{HG}^r \eta \sqrt{h_l^r}\left[h_{SH}^f s(t) + n_{SH}^u\right] + n_{HG}^u \tag{9}$$

$$\gamma_{HG}^r = \frac{\left(\eta h_{HG}^r \sqrt{h_l^r} h_{SH}^f m_0 P_t\right)^2}{\left(\eta h_{HG}^r \sqrt{h_l^r}\sigma_{n_{SH}^f}\right)^2 + \sigma_{n_{HG}^r}^2} \tag{10}$$

Where h_{HG}^r is the channel coefficient of the HAPS-to-GS RF link, n_{HG}^r is the AWGN with variance $\sigma_{n_{HG}^r}^2$, h_l^r is the path loss defined as [35]

$$h_l^r\,[\text{dB}] = G_T + G_R - 20\log_{10}\left(\frac{4\pi L_0}{f}\right) - \omega_{oxy}L_0 - \omega_{rain}L_0 \tag{11}$$

where G_T is the transmitter antenna gain (in dB), G_R is the receiver antenna gain (in dB), f is the RF frequency (in GHz), L_0 is the distance between HAPS and GS (in km), ω_{oxy} and ω_{rain} are the attenuation coefficients due to the oxygen absorption and rain scattering, respectively.

B. Satellite-to-HAP FSO Link

For the satellite-to-HAP FSO link, the channel coefficient h_{SH}^{f} can be given by $h_{SH}^{f} = h_{SH}^{l} h_{SH}^{p} h_{SH}^{a}$, where h_{SH}^{l} indicates the atmospheric attenuation, h_{SH}^{p} defines the pointing error, and h_{SH}^{a} is the atmospheric turbulence. Due to the absorption and scattering by particles in the atmosphere, optical beam will experience power loss during the propagation, which can be described by Beers-Lambert law as

$$h_{SH}^{l} = \exp(-\alpha_0 L_1) \tag{12}$$

Where L_1 is the length of FSO link between satellite and HAPS, α_0 represents the weather dependent attenuation coefficient [31, Eq. (16)]

$$\alpha_0 = \frac{3.91}{V\,[\text{km}]} \left(\frac{\lambda\,[\text{nm}]}{550} \right)^{-q_0} \tag{13}$$

Where λ is the optical wavelength, V is the visibility, q_0 is the size distribution of the scattering particles given by Kim model [37]. The pointing error is mainly caused by the laser beam displacement along elevation and azimuth which can be modeled as independent and identical Gaussian distributions expressed as $h_{SH}^{p} = A_0 \exp(-2r_0^2/\omega_e^2)$. Where A_0 is the fraction of the collected power at beam center, r_0 is the radial displacement between beam center and detector center, ω_e is the equivalent beam waist at the receiver [38]. And the probability density (PDF) of the irradiance h_{SH}^{p} is given by [39, eq. (11)]

$$f_{h_{SH}^{p}}(h_{SH}^{p}) = \frac{\xi_1^2}{A_0^{\xi_1^2}} (h_{SH}^{p})^{\xi_1^2 - 1}, 0 \le h_{SH}^{p} \le A_0 \tag{14}$$

Where ξ_1 is the ratio between the equivalent beam radius and the jitter standard deviation at the receiver, which is used to quantify the severity of the pointing error effect [39]. The atmospheric turbulence is modeled by Gamma-Gamma distribution due to its wide acceptance in the current literature, whose PDF is given in [40] as

$$f_{h_{SH}^{a}}(h_{SH}^{a}) = \frac{2(\alpha_1\beta_1)^{\frac{\alpha_1+\beta_1}{2}}}{\Gamma(\alpha_1)\Gamma(\beta_1)} (h_{SH}^{a})^{\frac{\alpha_1+\beta_1}{2}-1} K_{\alpha_1-\beta_1}(2\sqrt{\alpha_1\beta_1 h_{SH}^{a}}), h_{SH}^{a} > 0 \tag{15}$$

Depending on the atmospheric conditions, the scintillation parameters α_1 and β_1 are calculated as shown in Appendix A. Then, the combined PDF h_{SH}^{f} can be written in terms of Meijer G-function $G_{p,q}^{m,n}(\cdot)$ which is defined in [41, eq. (9.301)], and [42, 07.34.02.0001.01], and given as [23, eq. (10)]

$$f_{h_{SH}^{f}}(h_{SH}^{f}) = \frac{\xi_1^2 \alpha_1 \beta_1}{A_0 h_{SH}^{l} \Gamma(\alpha_1)\Gamma(\beta_1)} G_{1,3}^{3,0} \left[\frac{\alpha_1\beta_1}{A_0 h_{SH}^{l}} h_{SH}^{f} \middle| \begin{matrix} \xi_1^2 \\ \xi_1^2 - 1, \alpha_1 - 1, \beta_1 - 1 \end{matrix} \right] \tag{16}$$

The PDF of the instantaneous SNR of FSO links can be obtained from (16) using the power transformation of random variable and the resultant unified PDF expression is given as [43, eq. (4)]

$$f_{\gamma_{SH}^{f}}\left(\gamma_{SH}^{f}\right) = \frac{\xi_1^2}{b_1 \gamma_{SH}^{f} \Gamma(\alpha_1)\Gamma(\beta_1)} G_{1,3}^{3,0} \left[\frac{\alpha_1\beta_1\xi_1^2}{\xi_1^2+1} \left(\frac{\gamma_{SH}^{f}}{\mu_1} \right)^{\frac{1}{b_1}} \middle| \begin{matrix} \xi_1^2 + 1 \\ \xi_1^2, \alpha_1, \beta_1 \end{matrix} \right] \tag{17}$$

Where $\mu_1 = \bar{\gamma}_{SH}^{f}$ for heterodyne detection and $\mu_1 = \frac{(\xi_1^2+2)\alpha_1\beta_1\xi_1^2}{(\xi_1^2+1)^2(\alpha_1+1)(\beta_1+1)} \bar{\gamma}_{SH}^{f}$ for IM/DD detection, $b_1 = 1$ for HD detection and $b_1 = 2$ for IM/DD detection. The cumulative distribution function (CDF) of γ_{SH}^{f} can be obtained from (17) by using [42, eq. (07.34.21.0084.01)] given as

$$F_{\gamma_{SH}^{f}}(\gamma_{SH}^{f}) = F^1 G_{b_1+1,3b_1+1}^{3b_1,1} \left(\frac{D_1^{b_1} \gamma_{SH}^{f}}{b_1^{2b_1}\mu_1} \middle| \begin{matrix} 1 & E_1 \\ E_2 & 0 \end{matrix} \right) \tag{18}$$

Where $F^1 = \frac{\xi_1^2 b_1^{\alpha_1+\beta_1-2}}{(2\pi)^{b_1-1}\Gamma(\alpha_1)\Gamma(\beta_1)}$, $D_1 = \frac{\alpha_1\beta_1\xi_1^2}{\xi_1^2+1}$, $E_2 = \left\{ \frac{\xi_1^2}{b_1}, \ldots, \frac{\xi_1^2+b_1-1}{b_1}, \ldots, \frac{\alpha_1}{b_1}, \ldots, \frac{\alpha_1+b_1-1}{b_1}, \frac{\beta_1}{b_1}, \ldots, \frac{\beta_1+b_1-1}{b_1} \right\}$, $E_1 = \left\{ \frac{\xi_1^2+1}{b_1}, \ldots, \frac{\xi_1^2+b_1}{b_1} \right\}$. Mode 1 is adopted in cloudless weather where FSO link is in good quality. For mode 1, we assume the HAP-to-GS FSO link follows the same distribution with the satellite-to-HAP link but with different parameters α_2, β_2, ξ_2. $\alpha_1 > \alpha_2$, $\beta_1 > \beta_2$ are assumed due to the fact that the HAP-to-GS FSO link is more affected by atmospheric turbulence. $\xi_1 < \xi_2$ is assumed due to the movement of satellite. The CDF γ_{HG}^{f} of HAP-to-GS FSO link is given by

$$F_{\gamma_{HG}^{f}}(\gamma_{HG}^{f}) = F^2 G_{b_2+1,3b_2+1}^{3b_2,1} \left(\frac{D_2^{b_2} \gamma_{HG}^{f}}{b_2^{2b_2}\mu_2} \middle| \begin{matrix} 1 & E_3 \\ E_4 & 0 \end{matrix} \right) \tag{19}$$

Where $b_2 = 1$ for HD detection and $b_2 = 2$ for IM/DD detection, $F^2 = \frac{\xi_2^2 b_2^{\alpha_2+\beta_2-2}}{(2\pi)^{b_2-1}\Gamma(\alpha_2)\Gamma(\beta_2)}$, $D_2 = \frac{\alpha_2\beta_2\xi_2^2}{\xi_2^2+1}$, $E_4 = \left\{ \frac{\xi_2^2}{b_2}, \ldots, \frac{\xi_2^2+b_2-1}{b_2}, \ldots, \frac{\alpha_2}{b_2}, \ldots, \frac{\alpha_2+b_2-1}{b_2}, \frac{\beta_2}{b_2}, \ldots, \frac{\beta_2+b_2-1}{b_2} \right\}$, $E_3 = \left\{ \frac{\xi_2^2+1}{b_2}, \ldots, \frac{\xi_2^2+b_2}{b_2} \right\}$. $\mu_2 = \bar{\gamma}_{HG}^{f}$ for heterodyne detection and $\mu_2 = \frac{(\xi_2^2+2)\alpha_2\beta_2\xi_2^2}{(\xi_2^2+1)^2(\alpha_2+1)(\beta_2+1)} \bar{\gamma}_{HG}^{f}$ for IM/DD detection.

C. HAP-to-GS RIS Assisted UAV FSO Link

The HAP-to-GS RIS assisted UAV FSO link is adopted when mode 1 is unavailable due to clouds obstruction. For the HAP-to-GS RIS assisted UAV FSO link, h_{HG}^{u} can be given by $h_{HG}^{u} = h_l^u h_p^u h_a^u h_{aoa}^u$, where h_l^u indicates the atmospheric attenuation, h_p^u defines the average pointing error, h_a^u is the average atmospheric turbulence, and h_{aoa}^u is the link interruption due to AOA fluctuation. h_l^u is given by $h_l^u = \sum_{i=1}^{N} h_{li}^u u_i g_{li}^u$, where N is the number of reflecting meta-surfaces of the RIS, $h_{li}^u = \exp(\alpha_0 L_2)\exp(-j\theta_i)$ and $g_{li}^u = \exp(\alpha_0 L_3)\exp(-j\varphi_i)$ are the channel gains of the HAPS-to-RIS FSO link and RIS-to-GS FSO link, respectively. L_2 and L_3 are the length of two links. $u_i = \rho(\phi_i)e^{j\phi_i}$ is the reflection coefficient induced by the ith reflector of the RIS. Considering the UAV hovering-induced misalignment. h_p^u can be obtained from (14) by replacing h_{SH}^{p}, ξ_1^2 with h_p^u, ξ_3^2. Similarly, h_a^u can be obtained from (15) by

substituting h_{SH}^{a}, α_1, β_1 with h_{a}^{u}, α_3, β_3. Similar to mode 1, we assume that $\alpha_1 > \alpha_3$, $\beta_1 > \beta_3$, $\xi_1 < \xi_3$.

Due to the relatively large orientation deviations of hovering UAV, the incident laser arrives with θ_a at the receiving plane may be out of detector range occasionally, where θ_a is the AOA. According to [28], θ_a can be modeled as Rayleigh-distributed with zero mean and variance $\sigma_{angle,u}^{2}$ expressed as

$$f_{\theta_a}(\theta_a) = \frac{\theta_a}{\delta_{angle,u}^{2}} \exp\left(-\frac{\theta_a^2}{2\delta_{angle,u}^{2}}\right) \tag{20}$$

Considering the 0-1 distribution that describes whether the incident laser is located on the receiving field-of-view (FoV) or not. With a fixed θ_{FoV}, the FSO link will be in outage ($h_{aoa}^{u} = 0$) when $\theta_a > \theta_{FoV}$, and the maximum signal power ($h_{aoa}^{u} = 1$) is collect otherwise. The PDF of h_{aoa}^{u} is given as [28]

$$\begin{aligned} f_{h_{aoa}^{u}}(h_{aoa}^{u}) = {} & \exp\left(-\frac{\theta_{FoV}^2}{2\sigma_{angle,u}^{2}}\right)\delta(h_{aoa}^{u}) \\ & + \left[1 - \exp\left(-\frac{\theta_{FoV}^2}{2\sigma_{angle,u}^{2}}\right)\right]\delta(h_{aoa}^{u} - 1) \end{aligned} \tag{21}$$

Based on the above analysis, the PDF of h_{HG}^{u} can be expressed as

$$\begin{aligned} f_{h_{HG}^{u}}(h_{HG}^{u}) = {} & \exp\left(-\frac{\theta_{FoV}^2}{2\sigma_{angle,u}^{2}}\right)\delta(h_{HG}^{u}) \\ & + \left[1 - \exp\left(-\frac{\theta_{FoV}^2}{2\sigma_{angle,u}^{2}}\right)\right] \\ & \times \frac{\xi_3^2 \alpha_3 \beta_3}{A_0 h_l^{u} \Gamma(\alpha_3)\Gamma(\beta_3)} G_{1,3}^{3,0} \\ & \left[\frac{\alpha_3 \beta_3}{A_0 h_l^{u}} h_{HG}^{u} \middle| \begin{matrix} \xi_3^2 \\ \xi_3^2 - 1, \alpha_3 - 1, \beta_3 - 1 \end{matrix}\right] \end{aligned} \tag{22}$$

Therefore, the PDF of the instantaneous SNR of RIS assisted UAV FSO links can be obtained from (22) using the power transformation of random variable expressed as

$$\begin{aligned} f_{\gamma_{HG}^{u}}(\gamma_{HG}^{u}) = {} & \exp\left(-\frac{\theta_{FoV}^2}{2\sigma_{angle,u}^{2}}\right) + \left[1 - \exp\left(-\frac{\theta_{FoV}^2}{2\sigma_{angle,u}^{2}}\right)\right] \\ & \times \frac{\xi_3^2}{b_3 \gamma_{HG}^{u} \Gamma(\alpha_3)\Gamma(\beta_3)} \\ & \times G_{1,3}^{3,0}\left[\frac{\alpha_3 \beta_3 \xi_3^2}{\xi_3^2 + 1}\left(\frac{\gamma_{HG}^{u}}{\mu_3}\right)^{\frac{1}{b_3}} \middle| \begin{matrix} \xi_3^2 + 1 \\ \xi_3^2, \alpha_3, \beta_3 \end{matrix}\right] \end{aligned} \tag{23}$$

Where $b_3 = 1$ for HD detection and $b_3 = 2$ for IM/DD detection. The CDF of γ_{HG}^{u} can be obtained from (23) by using [43, eq. (07.34.21.0084.01)] given as

$$\begin{aligned} F_{\gamma_{HG}^{u}}(\gamma_{HG}^{u}) = {} & \exp\left(-\frac{\theta_{FoV}^2}{2\sigma_{angle,u}^{2}}\right) + \left[1 - \exp\left(-\frac{\theta_{FoV}^2}{2\sigma_{angle,u}^{2}}\right)\right] \\ & \times F^3 G_{b_3+1,3b_3+1}^{3b_3,1}\left(\frac{D_3^{b_3}\gamma_{HG}^{f}}{b_3^{2b_3}\mu_3} \middle| \begin{matrix} 1 & E_5 \\ E_6 & 0 \end{matrix}\right) \end{aligned} \tag{24}$$

Where $D_3 = \frac{\alpha_3\beta_3\xi_3^2}{\xi_3^2+1}$, $F^3 = \frac{\xi_3^2 b_3^{\alpha_3+\beta_3-2}}{(2\pi)^{b_3-1}\Gamma(\alpha_3)\Gamma(\beta_3)}$, $E_6 = \left\{\frac{\xi_3^2}{b_3}, \ldots, \frac{\xi_3^2+b_3-1}{b_3}, \ldots, \frac{\alpha_3}{b_3}, \ldots, \frac{\alpha_3+b_3-1}{b_3}, \frac{\beta_3}{b_3}, \ldots, \frac{\beta_3+b_3-1}{b_3}\right\}$ $E_5 = \left\{\frac{\xi_3^2+1}{b_3}, \ldots, \frac{\xi_3^2+b_3}{b_3}\right\}$, $\mu_3 = \bar{\gamma}_{HG}^{u}$ for heterodyne detection and $\mu_3 = \frac{(\xi_3^2+2)\alpha_3\beta_3\xi_3^2}{(\xi_3^2+1)^2(\alpha_3+1)(\beta_3+1)}\bar{\gamma}_{HG}^{u}$ for IM/DD detection.

D. HAP-to-GS RF Link

The HAP-to-GS RF link is adopted when other modes are unavailable, such as thick cloud or heavy fog weather. The RF link is assumed to follow the shadowed Rician model which fits well with land mobile satellite (LMS) channel model. The PDF of h_{HG}^{r} is given as [44, eq. (3)]

$$\begin{aligned} f_{h_{HG}^{r}}(h_{HG}^{r}) = {} & \frac{h_{HG}^{r}}{b}\left(\frac{2bm}{2bm+\Omega}\right)^{m} e^{-\frac{(h_{HG}^{r})^2}{2b}} \\ & \times \Phi_1\left(m; 1; \frac{1}{2b}\left(\frac{\Omega}{2bm+\Omega}\right)(h_{HG}^{r})^2\right), h_{HG}^{r} \geq 0 \end{aligned} \tag{25}$$

Where m represents the Nakagami-m severity parameter, Ω and $2b$ are the average power of the LOS component and multipath component, Φ_1 is the confluent hypergeometric function defined in [41, eq. (9.26)]. When m is an arbitrary positive real number, The CDF of shadowed Rician channel can be expressed as [45, (eq. (8)]

$$F_{h_{HG}^{r}}(h_{HG}^{r}) = k_0 h_{HG}^{r} \Phi_2\left(1-m, m; 2; -\frac{1}{2b}h_{HG}^{r}, -\varphi h_{HG}^{r}\right) \tag{26}$$

Where Φ_2 is the bivariate confluent hypergeometric function defined in [41, eq. (9.26)], $k_0 = \frac{1}{2b}\left(\frac{2bm}{2bm+\Omega}\right)^{m}$, and $\varphi = \frac{m}{2bm+\Omega}$. According to (25), the PDF of γ_{HG}^{r} can be given by using [42, eq. (07.20.03.0009.01)] and then [42, eq. (07.02.03.0014.01)] as

$$\begin{aligned} f_{\gamma_{HG}^{r}}(\gamma_{HG}^{r}) = {} & \frac{m}{\bar{\gamma}_{HG}^{r}}\left(\frac{2bm}{2bm+\Omega}\right)^{m-1} \exp\left(-\frac{m\gamma_{HG}^{r}}{\bar{\gamma}_{HG}^{r}}\right) \\ & \times \sum_{k=0}^{m-1} \frac{(-1)^k (1-m)_k}{k!^2}\left(\frac{\Omega\gamma_{HG}^{r}}{2b\bar{\gamma}_{HG}^{r}}\right)^{k} \end{aligned} \tag{27}$$

And the CDF of γ_{HG}^{r} is derived from (27) by applying [41, eq. (3.351/2)] given as

$$\begin{aligned} F_{\gamma_{HG}^{r}}(\gamma_{HG}^{r}) = {} & 1 - \left(\frac{2bm}{2bm+\Omega}\right)^{m-1} \exp\left(-\frac{m\gamma_{HG}^{r}}{\bar{\gamma}_{HG}^{r}}\right) \\ & \times \sum_{k=0}^{m-1} \frac{(-1)^k (1-m)_k}{k!}\left(\frac{\Omega}{2bm}\right)^{k} \sum_{j=0}^{k} \frac{1}{j!}\left(\frac{m\gamma_{HG}^{r}}{\bar{\gamma}_{HG}^{r}}\right)^{j} \end{aligned} \tag{28}$$

TABLE I
WEATHER-DEPENDENT LINK SELECTION SCHEME

Mode	Weather condition	Description	Link selection
Mode-1	Clear weather	FSO link is in better condition	HAPS relay FSO/FSO link
Mode-2	Rainy Weather	RF link is in worse condition	HAPS relay FSO/FSO link
Mode-3	Cloud Weather	Line-of-sight FSO link is blocked	RIS assisted UAV relay FSO link
Mode-4	Foggy Weather	FSO link is in worse condition	HAPS relay FSO/RF link

E. Links Switching Scheme Design

The HAPS is deployed with weather sensors which can detect the ground weather conditions and adapt to different transmission modes flexibly. Our proposed weather-dependent link selection scheme is summarized in Table I. The channel state information (CSI) conditions refer to the instantaneous SNR of the received signal, and the CSI conditions in the HAPS can be obtained through a 2-bit feedback signal from the GS and different transmission modes will be selected based on the received feedback signal. Firstly, the signal is directly transmitted from satellite to HAPS as this link is less effected by weather conditions. Then for mode 1, we consider clear weather condition and the FSO signal is directly transmitted to GS due to the availability and high-speed of FSO link. For mode 2, we consider the rainy weather where the FSO link is selected due to the huge rain attenuation of the RF link. For mode 3, the cloud weather is considered where the LOS link is unavailable and the FSO signal is firstly forwarded to the UAV and then reflected to the GS by the RIS. For mode 4, the foggy weather is considered and the RF link is selected due to the huge fog attenuation of the FSO link, and the optical signal is firstly converted into electrical signal by a photodiode in the HAPS, and then forwarded to the GS.

III. PERFORMANCE EVALUATION

In this section, we perform an analysis of the outage probability, average BER and ergodic capacity of our proposed system, and derive their closed form expressions which are in terms of bivariate Fox's H function and bivariate Meijer's G function.

A. Outage Probability

The outage probability is defined as that the instantaneous SNR falls below a predefined SNR, and for different modes, it can be expressed as $P_{out,k}(\gamma_{th}) = \Pr[\gamma \leq \gamma_{th}]$, for $k \in \{1,2,3,4\}$. The expression of $P_{out,k}(\gamma_{th})$ is given as

$$P_{out,k}(\gamma_{th}) = F_{\gamma_k}(\gamma_{th}) \tag{29}$$

Where $F_{\gamma_k}(\cdot)$ is the CDF of overall SNR under different working modes. The overall SNR of the mode 1 under AF scheme with a fixed relay gain Q can be expressed as $\gamma = \frac{\gamma_{SH}^f \gamma_{HG}^f}{\gamma_{HG}^f + Q}$. Therefore, the CDF of overall SNR of mode 1 is given as

$$F_{\gamma_1}(\gamma) = F_{\gamma_{SH}^f}(\gamma) - \frac{\xi_1^2 F^2}{b_1 \Gamma(\alpha_1)\Gamma(\beta_1)} H_{1,0:3,2:b_2,3b_2+1}^{0,1:0,3:3b_2+1,0}$$

$$\left[\begin{array}{c|c|c|c} (1,1,1/b_1) & & & \\ - & & & \\ \left(1-\xi_1^2,1\right),\left(1-\alpha_1,1\right),\left(1-\beta_1,1\right) & \dfrac{\xi_1^2+1}{\alpha\beta\xi_1^2}\left(\dfrac{\mu_1}{\gamma}\right)^{\frac{1}{b_1}}, \dfrac{D_2^{b_2}Q}{b_2^{2b_2}\mu_2} \\ \left(-\xi_1^2,1\right),(0,1/b_1) & & & \\ (E_3,1) & & & \\ (E_4,1),(0,1/b_2) & & & \end{array}\right] \tag{30}$$

Proof: Please refer to Appendix B.

Where $H_{\cdot,\cdots,\cdot}^{\cdot,\cdots,\cdot}(\cdot,\cdot)$ is the bivariate Fox's H function, and when both FSO links are operating under heterodyne detection, i.e., $b_1 = b_2 = 1$, (30) can be simplified in terms of the extended generalized bivariate Meijer's G function $G_{\cdot,\cdots,\cdot}^{\cdot,\cdots,\cdot}(\cdot,\cdot)$ expressed as

$$F_{\gamma_1}(\gamma) = F_{\gamma_{SH}^f}(\gamma) - \frac{\xi_1^2 F^2}{b_1 \Gamma(\alpha_1)\Gamma(\beta_1)} G_{1,0:3,2:b_2,3b_2+1}^{0,1:0,3:3b_2+1,0}$$

$$\left[\begin{array}{c|c|c|c} 1 & 1-\xi_1^2, 1-\alpha_1, 1-\beta_1 & E_3 & \dfrac{\xi_1^2+1}{\alpha_1\beta_1\xi_1^2}\left(\dfrac{\mu_1}{\gamma}\right)^{\frac{1}{b_1}}, \dfrac{D_2^{b_2}Q}{b_2^{2b_2}\mu_2} \\ - & -\xi_1^2, 0 & E_4, 0 & \end{array}\right] \tag{31}$$

Therefore, the outage probability of mode 1 under heterodyne detection can be expressed as

$$P_{out,1}(\gamma_{th}) = F_{\gamma_{SH}^f}(\gamma_{th}) - \frac{\xi_1^2 F^2}{b_1 \Gamma(\alpha_1)\Gamma(\beta_1)} G_{1,0:3,2:b_2,3b_2+1}^{0,1:0,3:3b_2+1,0}$$

$$\left[\begin{array}{c|c|c|c} 1 & 1-\xi_1^2, 1-\alpha_1, 1-\beta_1 & E_3 & \dfrac{\xi_1^2+1}{\alpha_1\beta_1\xi_1^2}\left(\dfrac{\mu_1}{\gamma_{th}}\right)^{\frac{1}{b_1}}, \dfrac{D_2^{b_2}Q}{b_2^{2b_2}\mu_2} \\ - & -\xi_1^2, 0 & E_4, 0 & \end{array}\right] \tag{32}$$

Due to different weather attenuation coefficients, mode 2 has the same expression as mode 1 but different average SNR μ_2. Similarly, the outage probability of mode 3 under heterodyne detection can be obtained in the same way as mode 1 given as

$$P_{out,3}(\gamma_{th}) = \exp\left(-\frac{\theta_{FoV}^2}{2\sigma_{angle,u}^2}\right) + \left(1 - \exp\left(-\frac{\theta_{FoV}^2}{2\sigma_{angle,u}^2}\right)\right)$$

$$\times \left(F_{\gamma_{SH}^f}(\gamma_{th}) - \frac{\xi_1^2 F^3}{b_1 \Gamma(\alpha_1)\Gamma(\beta_1)} G_{1,0:3,2:b_3,3b_3+1}^{0,1:0,3:3b_3+1,0}\right.$$

$$\left.\left[\begin{array}{c|c|c|c} 1 & 1-\xi_1^2, 1-\alpha_1, 1-\beta_1 & E_5 & \dfrac{\xi_1^2+1}{\alpha_1\beta_1\xi_1^2}\left(\dfrac{\mu_1}{\gamma_{th}}\right)^{\frac{1}{b_1}}, \dfrac{D_3^{b_3}Q}{b_3^{2b_3}\mu_3} \\ - & -\xi_1^2, 0 & E_6, 0 & \end{array}\right]\right) \tag{33}$$

For mode 4, we consider the CSI-assisted relaying with gain C, so the outage probability of mode 4 is given as

$$P_{out,4}(\gamma_{th}) = 1 - \frac{\xi_1^2 b_1^{\alpha_1+\beta_1-2}}{\Gamma(\alpha_1)\Gamma(\beta_1)(2\pi)^{b_1-1}} \left(\frac{2bm}{2bm+\Omega}\right)^{m-1}$$

$$\times \sum_{k=0}^{m-1}\sum_{j=0}^{k} \frac{(-1)^k (1-m)_k}{k!j!} \times \left(\frac{\Omega}{2bm}\right)^k \times G_{1,0:0,2:3b_1,b_1+1}^{0,1:2,0:0,3b_1}$$

$$\left[\begin{array}{c|c|c|c} 0 & - & K_1 & \dfrac{Cm}{\bar{\gamma}_{HG}^r}, \dfrac{b_1^{2b_1}\left(\xi_1^2+1\right)^{b_1}\mu_1}{\left(\alpha_1\beta_1\xi_1^2\right)^{b_1}\gamma_{th}} \\ & j, 1 & \Delta(b_1, -\xi_1^2), 0 & \end{array}\right] \tag{34}$$

Proof: Please refer to Appendix C.

TABLE II
PARAMETERS FOR DIFFERENT MODULATION SCHEMES

Modulation	δ	p	q_u	n	Detection Type
OOK	1	0.5	0.5	1	IM/DD
BPSK	1	0.5	1	1	Heterodyne
M-PSK	$\frac{2}{\max(\log_2 M,2)}$	0.5	$\sin^2\left(\frac{(2u-1)\pi}{M}\right)$	$\max\left(\frac{M}{4},1\right)$	Heterodyne
M-QAM	$\frac{4}{\log_2 M}\left(1-\frac{1}{\sqrt{M}}\right)$	0.5	$\frac{3(2u-1)^2}{2(M-1)}$	$\frac{\sqrt{M}}{2}$	Heterodyne

The average outage probability of our proposed system can be expressed as $P_{out}(\gamma_{th}) = \sum_{k=1}^{4} p_k P_{out,k}(\gamma_{th})$, where p_k is the probability that the kth mode is selected.

B. Average Bit-Error Rate Performance

The average BER for different modulation schemes can be expressed as [23, eq. (46)]

$$P_e = \frac{\sigma}{2\Gamma(p)} \sum_{u=1}^{n} q_u^p \int_0^\infty x^{p-1} e^{-q_u x} F_i(x)\, dx \tag{35}$$

Where n, σ, p, and q_u vary depending on the type of detection and modulation technique which can be found in Table II at the top of next page.

Substituting (B.5) into (35), and by using [41, eq. (3.381/4)], then [47, eq. (1)], the average BER of mode 1 can be obtained as

$$P_{e,1} = \frac{\sigma}{2\Gamma(p)} F_p - \frac{\sigma \xi_1^2 F^2}{2b_1 \Gamma(\alpha_1)\Gamma(\beta_1)\Gamma(p)} H_{1,0:3,3:b_2,3b_2+1}^{0,1:1,3:3b_2+1,0} \left[\begin{matrix} (1,1,1/b_1) \\ - \\ \left(1-\xi_1^2,1\right),(1-\alpha_1,1),(1-\beta_1,1) \\ \left(p,\frac{1}{b_1}\right)\left(-\xi_1^2,1\right),(0,1/b_1) \\ (E_3,1) \\ (E_4,1),(0,1/b_2) \end{matrix} \middle| \frac{\xi_1^2+1}{\alpha\beta\xi_1^2}(q_u\mu_1)^{\frac{1}{b_1}}, \frac{D_2^{b_2}Q}{b_2^{2b_2}\mu_2} \right] \tag{36}$$

Proof: Please refer to Appendix D.

Similar to the analysis of outage probability, when we only consider heterodyne detection, the average BER of mode1 and mode 3 can be given by (37) and (38) shown at the bottom of this page, respectively.

$$P_{e,1} = \frac{\sigma F_p}{2\Gamma(p)} - \frac{\sigma \xi_1^2 F^2}{2b_1 \Gamma(\alpha_1)\Gamma(\beta_1)\Gamma(p)} \sum_{u=1}^{n} G_{1,0:3,3:b_2,3b_2+1}^{0,1:1,3:3b_2+1,0} \left[\begin{matrix} 1 \\ - \end{matrix} \middle| \begin{matrix} 1-\xi_1^2, 1-\alpha_1, 1-\beta_1 \\ p, -\xi_1^2, 0 \end{matrix} \middle| \begin{matrix} E_3 \\ E_4, 0 \end{matrix} \middle| \frac{(\xi_1^2+1)}{\alpha_1\beta_1\xi_1^2}(q_u\mu_1)^{\frac{1}{b_1}}, \frac{D_2^{b_2}Q}{b_2^{2b_2}\mu_2} \right] \tag{37}$$

The average BER of mode 2 has the same expression as mode 1 but different average SNR μ_2 due to different weather attenuation coefficients. Substituting (C.5) into (35), and by using [41, eq. (3.381/4)], then [48, eq. (1)], the average BER of mode 4 can be obtained as (39) shown at the bottom of this page.

Therefore, the average BER of our proposed system can be given as $P_e = \sum_{k=1}^{4} p_k P_{e,k}$.

C. Ergodic Capacity

Ergodic capacity is an important performance metric of wireless communication systems, which represents the time average of the maximum information rate of a random fading channel. The ergodic capacity of the both FSO link and RF link under HD and IM/DD techniques can be expressed as [33, eq. (34)]

$$\begin{aligned} \overline{C} &= E\left[\log_2(1+c\gamma)\right] \\ &= \frac{1}{\ln 2} \int_0^\infty \ln(1+c\gamma) f_\gamma(\gamma) d\gamma \end{aligned} \tag{40}$$

Where $c = 1$ for heterodyne technique and $c = e/(2\pi)$ for IM/DD technique. For mode 1, the ergodic capacity can be

$$P_{e,3} = \exp\left(-\frac{\theta_{FoV}^2}{2\sigma_{angle,u}^2}\right) + \left(1 - \exp\left(-\frac{\theta_{FoV}^2}{2\sigma_{angle,u}^2}\right)\right) \times \left(\frac{\sigma F_p}{2\Gamma(p)} - \frac{\sigma \xi_1^2 F^3}{2b_1\Gamma(\alpha_1)\Gamma(\beta_1)\Gamma(p)} \times \sum_{u=1}^{n} G_{1,0:3,3:b_2,3b_2+1}^{0,1:1,3:3b_2+1,0} \left[\begin{matrix} 1 \\ - \end{matrix} \middle| \begin{matrix} 1-\xi_1^2, 1-\alpha_1, 1-\beta_1 \\ p, -\xi_1^2, 0 \end{matrix} \middle| \begin{matrix} E_5 \\ E_6, 0 \end{matrix} \middle| \frac{(\xi_1^2+1)}{\alpha_1\beta_1\xi_1^2}(q_u\mu_1)^{\frac{1}{b_1}}, \frac{D_3^{b_3}Q}{b_3^{2b_3}\mu_3} \right] \right) \tag{38}$$

$$P_{e,4} = \frac{\sigma n}{2} - \frac{\sigma \xi_1^2 b_1^{\alpha_1+\beta_1-2}}{2\Gamma(\alpha_1)\Gamma(\beta_1)\Gamma(p)(2\pi)^{b_1-1}} \left(\frac{2bm}{2bm+\Omega}\right)^{m-1} \times \sum_{u=1}^{n} \sum_{k=0}^{m-1} \sum_{j=0}^{k} \frac{(-1)^k (1-m)_k}{k!j!} \left(\frac{\Omega}{2bm}\right)^k \times G_{1,0:0,2:3b_1,b_1+2}^{0,1:2,0:1,3b_1} \left[0 \middle| \begin{matrix} - \\ j,1 \end{matrix} \middle| \begin{matrix} K_1 \\ p, \Delta(b_1,-\xi_1^2), 0 \end{matrix} \middle| \frac{Cm}{\overline{\gamma}_{HG}^r}, \frac{b_1^{2b_1} q_u (\xi_1^2+1)^{b_1} \mu_1}{(\alpha_1\beta_1\xi_1^2)^{b_1}} \right] \tag{39}$$

expressed as equation (41) shown at the bottom of this page,

Proof: Please refer to Appendix E.

Similar to the analysis of average BER, when we only consider heterodyne detection, the ergodic capacity of mode1 and mode 3 can be given by (42) and (43) shown at the bottom of this page, respectively.

The ergodic capacity of mode 2 also has the same expression as mode 1 but different average SNR μ_2 due to different weather attenuation coefficients. Substituting (C.5) into (40), similar to the derivation process of mode 1, the ergodic capacity of mode 4 can be obtained as

$$\begin{aligned}\overline{C}_{EC,4} = &\frac{\xi_1^2 b_1^{\alpha_1+\beta_1-2}}{\Gamma(\alpha)\Gamma(\beta)(2\pi)^{b_1-1}}\left(\frac{2bm}{2bm+\Omega}\right)^{m-1}\\ &\times\sum_{k=0}^{m-1}\sum_{j=0}^{k}\frac{(-1)^k(1-m)_k}{k!j!}\left(\frac{\Omega}{2bm}\right)^k\\ &\times G_{1,0:0,2:3b_1+1,b_1+2}^{1,0:2,0:1,3b_1+1}\\ &\left[0\left|\begin{matrix}-\\ j,1\end{matrix}\right|\begin{matrix}1,K_1\\ 1,\Delta(b_1,-\xi_1^2),0\end{matrix}\left|\frac{Qm}{\bar{\gamma}_{HG}^r},\frac{b_1^{2b_1}c(\xi^2+1)^{b_1}\mu_1}{(\alpha_1\beta_1\xi_1^2)^{b_1}}\right.\right]\end{aligned} \tag{44}$$

Therefore, the ergodic capacity of our proposed system can be calculated by $\overline{C}_{EC} = \sum_{k=1}^{4} p_k \overline{C}_{EC,k}$.

IV. Asymptotic Analysis

In this section, we perform asymptotic analysis of the system outage probability and average BER under high SNR, the diversity order is also obtained to get more insights.

A. Asymptotic Outage Probability Analysis

Using [42, eq. (07.34.06.0040.01)], [47, eq. (1.1)] and [46, eq. (1.8.4)], the asymptotic outage probability of mode 1 is given by

$$\begin{aligned}P_{out,1}(\gamma_{th}) \overset{\mu_1,\mu_2\gg 1}{\approx} &F^1\sum_{k=1}^{3b_1}\\ &\frac{\prod_{\substack{j=1\\ j\neq k}}^{3b_1}\Gamma(E_{2j}-E_{2k})\Gamma(E_{2k})}{\prod_{j=2}^{b_1+1}\Gamma(E_{1j}-E_{2k})(1+E_{2k})}\left(\frac{D_1^{b_1}\gamma_{th}}{b_1^{2b_1}\mu_1}\right)^{E_{2k}}\\ &-\sum_{i=1}^{3}K_i\left[\left(\frac{\alpha_1\beta_1\xi_1^2}{\xi_1^2+1}\right)^{b_1}\frac{\gamma_{th}}{\mu_1}\right]^{G_{d1}^i}\\ &+\sum_{j=1}^{6}Z_j\left[\left(\frac{\alpha_1\beta_1\xi_1^2}{\xi_1^2+1}\right)^{b_1}\left(\frac{\alpha_2\beta_2\xi_2^2}{\xi_2^2+1}\right)^{b_2}\frac{Q\gamma_{th}}{\mu_1\mu_2}\right]^{G_{d1}^j}\end{aligned} \tag{45}$$

Where E_{2j} and E_{2k} mean the *j*th and *k*th term of E_2, E_{1j} means the *j*th term of E_1, $G_{d1} = (\frac{\alpha_1}{b_1}, \frac{\beta_1}{b_1}, \frac{\xi_1^2}{b_1}, \frac{\alpha_2}{b_2}, \frac{\beta_2}{b_2}, \frac{\xi_2^2}{b_2})$, K_i and Z_j are the polynomial about α_i, β_i, ξ_i, b_i (i.e., $i = 1, 2$), and their expressions are not given for simplicity, G_{d1}^i and G_{d1}^j mean the *i*th and *j*th term of G_{d1}. From (45), we can observe that

$$\begin{aligned}\overline{C}_{EC,1} = F_s + &\frac{\xi_1^2F^2}{b_1\Gamma(\alpha_1)\Gamma(\beta_1)}H_{1,0:4,3:b_2,3b_2+1}^{0,1:1,4:3b_2+1,0}\\ &\left[\begin{matrix}(1,1,1/b_1)\\ -\\ (1-\xi_1^2,1),(1-\alpha_1,1),(1-\beta_1,1),(1,1/b_1)\\ (1,1/b_1),(-\xi_1^2,1),(0,1/b_1)\\ (E_3,1)\\ (E_4,),(0,1)\end{matrix}\right|\left.\frac{\xi_1^2+1}{\alpha_1\beta_1\xi_1^2}(c\mu_1)^{\frac{1}{b_1}},\frac{D_2^{b_2}Q}{b_2^{2b_2}\mu_2}\right]\end{aligned} \tag{41}$$

$$\begin{aligned}\overline{C}_{EC,1} = F_s + &\frac{\xi_1^2F^2}{b_1\Gamma(\alpha_1)\Gamma(\beta_1)}G_{1,0:4,3:b_2,3b_2+1}^{0,1:1,4:3b_2+1,0}\\ &\left[\begin{matrix}1\\ -\end{matrix}\right|\left.\begin{matrix}1-\xi_1^2,1-\alpha_1,1-\beta_1,1\\ 1,-\xi_1^2,0\end{matrix}\right|\left.\begin{matrix}1+\xi_2^2\\ \xi_2^2,\alpha_2,\beta_2,0\end{matrix}\right|\left.\frac{\xi_1^2+1}{\alpha_1\beta_1\xi_1^2}(c\mu_1)^{\frac{1}{b_1}},\frac{D_2^{b_2}Q}{b_2^{2b_2}\mu_2}\right]\end{aligned} \tag{42}$$

$$\begin{aligned}\overline{C}_{EC,3} = &\exp\left(-\frac{\theta_{FoV}^2}{2\sigma_{angle,u}^2}\right)+\left(1-\exp\left(-\frac{\theta_{FoV}^2}{2\sigma_{angle,u}^2}\right)\right)\\ &\times\left(F_s+\frac{\xi_1^2F^2}{b_1\Gamma(\alpha_1)\Gamma(\beta_1)}\times G_{1,0:4,3:b_3,3b_3+1}^{0,1:1,4:3b_3+1,0}\right.\\ &\left.\left[\begin{matrix}1\\ -\end{matrix}\right|\left.\begin{matrix}1-\xi_1^2,1-\alpha_1,1-\beta_1,1\\ 1,-\xi_1^2,0\end{matrix}\right|\left.\begin{matrix}1+\xi_3^2\\ \xi_3^2,\alpha_3,\beta_3,0\end{matrix}\right|\left.\frac{\xi_1^2+1}{\alpha_1\beta_1\xi_1^2}(c\mu_1)^{\frac{1}{b_1}},\frac{D_3^{b_3}Q}{b_3^{2b_3}\mu_3}\right]\right)\end{aligned} \tag{43}$$

$P_{out,1}(\gamma_{th}) \propto (\mu_1)^{-G_{d1}}$ and $P_{out,1}(\gamma_{th}) \propto (\mu_2)^{-G_{d1}}$, the diversity of mode 1 is given by $G_1 = \min(\frac{\alpha_1}{b_1}, \frac{\beta_1}{b_1}, \frac{\xi_1^2}{b_1}, \frac{\alpha_2}{b_2}, \frac{\beta_2}{b_2}, \frac{\xi_2^2}{b_2})$. Due to $\alpha_1 > \alpha_2$, $\beta_1 > \beta_2$, $\xi_1 < \xi_2$ and assume that both FSO links use the same detection technology, the diversity of mode 1 can be expressed by $G_1 = \min(\frac{\alpha_2}{b_1}, \frac{\beta_2}{b_1}, \frac{\xi_1^2}{b_1})$. Similarly, the diversity of mode3 can be given as $G_3 = \min(\frac{\alpha_3}{b_1}, \frac{\beta_3}{b_1}, \frac{\xi_1^2}{b_1})$ under the assumption that $\alpha_1 > \alpha_3$, $\beta_1 > \beta_3$, $\xi_1^2 < \xi_3^2$. For mode 4, starting from (C.3), using [46, eq. (1.5.9)] and then [46, eq. (1.8.4)], the outage probability of mode 4 under high SNR can be written asymptotically as

$$P_{out,4}(\gamma_{th}) \overset{\mu_1 \to \infty}{\approx} 1 - \frac{\xi_1^2}{\Gamma(\alpha_1)\Gamma(\beta_1)} \left(\frac{2bm}{2bm+\Omega}\right)^{m-1} \times \sum_{k=0}^{m-1} \sum_{j=0}^{k} (-1)^k \times \frac{(1-m)_k}{k!j!} \left(\frac{\Omega}{2bm}\right)^k \times \sum_{i=1}^{4} J_i \left(\frac{\gamma_{th}}{\mu_1}\right)^{G_{d4}^i} \tag{46}$$

Where $G_{d4} = (j, \frac{\alpha_1}{b_1}, \frac{\beta_1}{b_1}, \frac{\xi_1^2}{b_1})$, G_{d4}^i means the ith term of G_{d4}, J_i is the polynomial about α_1, β_1, ξ_1, b_1. The diversity of mode 4 is given by $G_4 = \min(j, \frac{\alpha_1}{b_1}, \frac{\beta_1}{b_1}, \frac{\xi_1^2}{b_1})$. Therefore, the asymptotic outage probability of our proposed system is $G_{OP} = \min(G_1, G_3, G_4)$.

B. Asymptotic Average BER Analysis

Starting from (35), and similar to the asymptotic analysis of outage probability, the asymptotic average BER of mode 1 is given by

$$P_{e,1} \overset{\mu_1,\mu_2 \gg 1}{\approx} \frac{\sigma F^1}{2\Gamma(p)} \sum_{k=1}^{3b_1} \frac{\prod_{\substack{j=1 \\ j\neq k}}^{3b_1} \Gamma(E_{2j} - E_{2k}) \Gamma(E_{2k}) \Gamma(p + E_{2k})}{\prod_{j=2}^{b_1+1} \Gamma(E_{1j} - E_{2k})(1 + E_{2k})} \left(\frac{D_1^{b_1}\gamma_{th}}{b_1^{2b_1}\mu_1}\right)^{E_{2k}} - \sum_{i=1}^{3} X_i \sum_{k=1}^{n} \left[\left(\frac{\alpha_1\beta_1\xi_1^2}{\xi_1^2+1}\right)^{b_1} \frac{1}{q_k\mu_1}\right]^{V_{d1}^i} - \sum_{j=1}^{6} Y_j \sum_{k=1}^{n} \left[\left(\frac{\alpha_1\beta_1\xi_1^2}{\xi_1^2+1}\right)^{b_1} \left(\frac{\alpha_2\beta_2\xi_2^2}{\xi_2^2+1}\right)^{b_2} \frac{Q}{q_k\mu_1\mu_2}\right]^{V_{d1}^j} \tag{47}$$

Where $V_{d1} = (\frac{\alpha_1}{b_1}, \frac{\beta_1}{b_1}, \frac{\xi_1^2}{b_1}, \frac{\alpha_2}{b_2}, \frac{\beta_2}{b_2}, \frac{\xi_2^2}{b_2})$, X_i and Y_j are the polynomial about α_i, β_i, ξ_i, b_i (i.e., $i = 1, 2$). From (47), it can be observed that $P_{e,1} \propto (\mu_1)^{-V_{d1}}$ and $P_{e,1} \propto (\mu_2)^{-V_{d1}}$, thus the asymptotic average BER of mode 1 is given by $V_1 = \min(\frac{\xi_1^2}{b_1}, \frac{\alpha_2}{b_1}, \frac{\beta_2}{b_1})$. Similarly, the asymptotic average BER of mode 3 is given by $V_3 = \min(\frac{\xi_1^2}{b_1}, \frac{\alpha_3}{b_1}, \frac{\beta_3}{b_1})$. As for mode 4, the asymptotic average can be obtained by substituting the CDF at high SNR which can be obtained from (45), into (35), and using

TABLE III
SYSTEM PARAMETERS

Parameter	Value
Altitude of satellite, H_s	550 Km (LEO)
Altitude of HAPS, h_p	20 Km
Altitude of GS, h_g	0.8Km
Zenith angle, ς	30°
Wavelength, λ	1550nm
RF frequency band, f	40GHz
Conversion coefficient, η	80%
Fixed gain, Q	1.2
amplification factor, G_{FSO}	50dBi
HAPS antenna gain, G_T	45dBi
GS antenna gain, G_R	45dBi

[41, eq. (3.381/4)], shown as

$$P_{e,4} \overset{\mu_1 \gg 1}{\approx} \frac{\sigma n}{2} - \frac{\sigma\xi_1^2}{2\Gamma(\alpha_1)\Gamma(\beta_1)\Gamma(p)} \left(\frac{2bm}{2bm+\Omega}\right)^{m-1} \times \sum_{u=1}^{n} \sum_{k=0}^{m-1} \sum_{j=0}^{k} (-1)^k \times \frac{(1-m)_k}{k!j!} \left(\frac{\Omega}{2bm}\right)^k \times \sum_{i=1}^{4} J_i \Gamma\left(p + V_{d,3}^i\right) (q_u\mu_1)^{-V_{d4}^i} \tag{48}$$

Where $V_{d,4}$ has the same expression with $G_{d,4}$. Therefore, the asymptotic average BER of mode 4 is given by $V_4 = \min(j, \frac{\alpha_1}{b_1}, \frac{\beta_1}{b_1}, \frac{\xi_1^2}{b_1})$. The asymptotic average BER of our proposed system is $V_{ABER} = \min(V_1, V_3, V_4)$.

V. Number Results and Discussion

In this section, we evaluate the performance of our proposed system in terms of outage probability, average BER and ergodic capacity, and its correctness is verified by means of Monte Carlo simulations. The system parameters in our simulation are shown in Table III. The threshold SNR is set as $\gamma_{th} = 5$ dB unless otherwise specified, the rain rate is set as 12.5 mm/h and the oxygen scattering parameter is set as ω_{oxy}= 0.1 dB/km. For satellite-to-HAPS FSO link, we consider light turbulence $C_n^2(0) = 5 \times 10^{-13}$, α and β can be calculated from (A.1) and (A.2) as $(\alpha, \beta) = (5.76, 5.36)$ when beam wander effects are ignored. And for HAPS-to-GS FSO link, we consider two types of turbulence conditions, $C_n^2(0) = 1 \times 10^{-12}$ for moderate turbulence and $C_n^2(0) = 5 \times 10^{-12}$ for heavy turbulence. Hence, from (A.1) and (A.2), α and β can be calculated as$(\alpha, \beta) = (3.62, 3.29)$, $(\alpha, \beta) = (1.65, 1.36)$ when beam wander effects are ignored. For RF link, we consider the moderate shadowing $\{m, b, \Omega\} = (5, 0.251, 0.279)$ which is provided in [18], Table II. Moreover, without loss of generality, we assume that the different weather conditions have the same probability of occurrence and satisfy $\sum_{k=1}^{4} p_k = 1$. Therefore, the probability of different modes can be expressed as $p_k = 1/4$ for $k = 1, 2, 3, 4$. We also compare the performance of our proposed system with the existing schemes named FSO/FSO scheme and FSO/RF

TABLE IV
WEATHER-DEPENDENT VARIABLES

Weather condition	α_0 (dB/Km)	ω_{rain} (dB/Km)
Clear Weather	0.43	0.01
Rainy Weather	5.84	5.69
Cloud weather	3.34	0.1
Foggy Weather	16.67	0.1

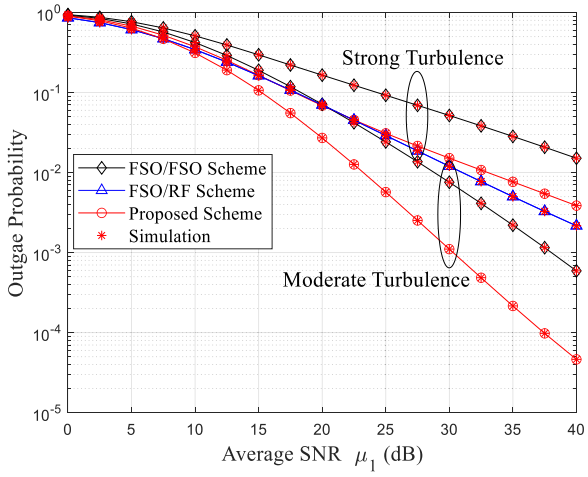

Fig. 2. Outage probability under different turbulence conditions using IM/DD technique.

scheme. In FSO/FSO scheme, both the links between satellite-to-HAPS and HAPS-to-GS are FSO links, while in FSO/RF scheme, the link between satellite-to-HAPS is FSO link and the link between HAPS-to-GS is RF link. In addition, the values of weather-dependent variables are tabulated in Table IV [49].

The outage probability of our proposed scheme under different turbulence conditions using IM/DD technique is plotted in Fig. 2. The average SNR of HAP-to-GS link is assumed as 20 dB. The analytical results provide a perfect match to the simulation results which prove the accuracy of our derivation. It can be observed that the outage performance improves with the increase of average SNR of satellite-to-HAPS FSO link. The performance of FSO/FSO scheme severely deteriorates under strong turbulence conditions compared to FSO/RF scheme and our proposed scheme, which is due to the fact that strong turbulence can lead to a severe decrease in the availability of FSO link and our proposed scheme can flexibly switch to the RF link to avoid it. As we assume that the satellites-to-HAPS link is almost unaffected by turbulence, so the FSO/RF scheme is not affected by turbulence conditions. Moreover, our proposed scheme can achieve significant advantage under moderate turbulence which attribute to the better availability of both FSO link and RF link provides more switching options. Hence, our proposed scheme can achieve better outage performance than FSO/FSO scheme especially in moderate turbulence conditions, and is slightly inferior to FSO/RF scheme in strong turbulence. In a nutshell, our proposed scheme owns superiority in both stability and reliability.

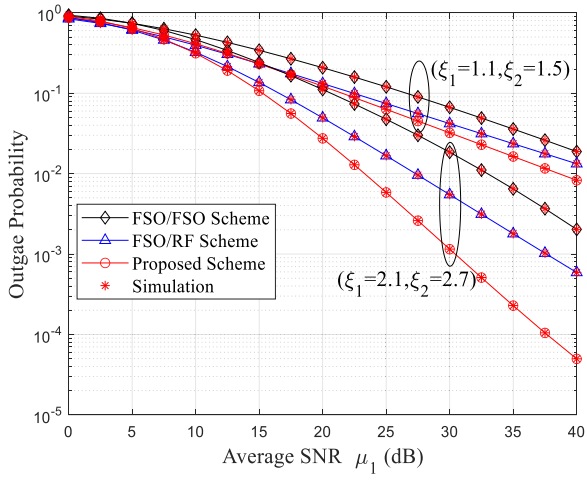

Fig. 3. Outage probability under different pointing errors using IM/DD technique.

The outage performance of our proposed scheme in operation under IM/DD technique with different pointing errors is illustrated in Fig. 3. ξ_1 means the pointing error of the satellite-to-HAPS FSO link while ξ_2 means the pointing error of the HAP-to-GS FSO link. We can observe that the outage performance can be improved by increasing the pointing error parameter ξ. This is due to the fact that a larger value of ξ can reduce the effect of beam jitter. Hence, the outage performance of both satellite-to-HAPS FSO link and HAPS-to-GS FSO link can be improved. It can also be found that our proposed scheme can achieve better outage performance compared to FSO/FSO scheme and FSO/RF scheme under different pointing errors. For example, at SNR $= 30$ dB, for $\xi_1 = 2.1$, $\xi_2 = 2.7$, the outage probability of our proposed scheme is $P_{\text{out}} = 1.15 \times 10^{-3}$, and it increases to 5.48×10^{-3} and 1.85×10^{-2} for FSO/RF scheme and FSO/FSO scheme, respectively, which is due to the fact that the FSO/RF scheme will severely deteriorate in rainy weather while FSO/FSO scheme will face performance degradation in foggy weather. However, our proposed switching strategy can avoid degradation by selecting different transmission modes. Moreover, our proposed scheme owns significant advantages with higher values of ξ, which is due to that the improvement of FSO link provides more switching options.

Fig. 4 depicts the outage probability using both IM/DD and HD technique under different pointing errors. We can observe that HD technique can achieve a considerable improvement of outage performance compared to IM/DD technique, especially in cases of good pointing error. Due to the advantage of better spectral efficiency and higher sensitivity, HD technique can be a better choice to overcome the pointing errors and turbulence effects, at the cost of higher complexity. Interestingly, we can find that the outage performance under HD technique with good pointing error tends to a saturation as μ_1 continues increasing. This can be attributed to the fact that the outage performance is limited by maximum transmit power of HAPS and the fixed interruption probability caused by AOA fluctuation. Consequently, the deployment of RIS assisted UAV relay can provide spatial diversity which can to some extent improve system performance.

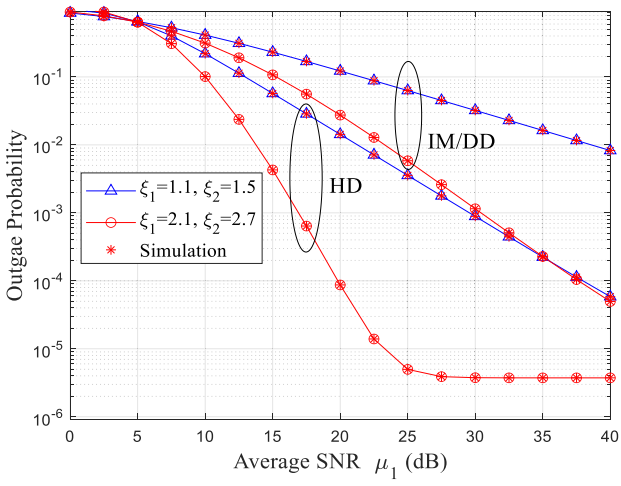

Fig. 4. Outage probability using both IM/DD and HD technique under different pointing errors.

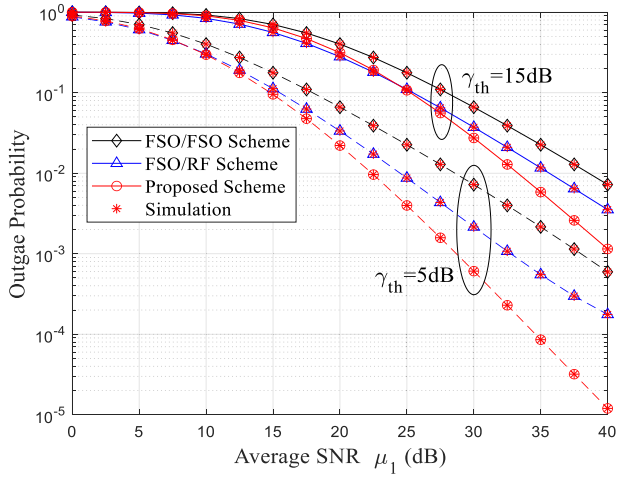

Fig. 5. Outage probability under different threshold SNR using IM/DD technique.

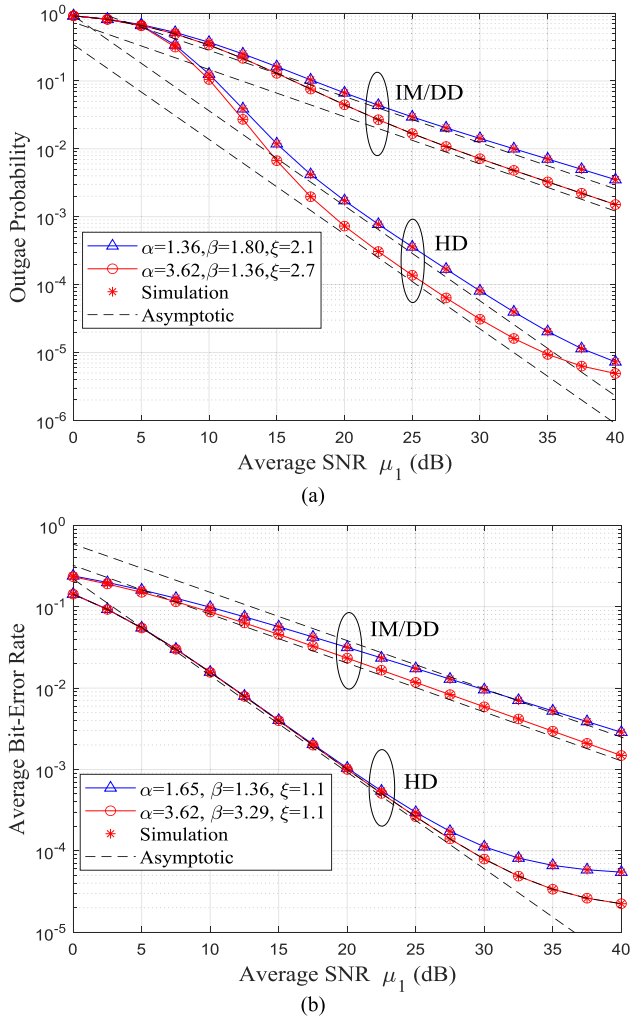

Fig. 6. (a) Asymptotic outage performance analysis under both HD and IM/DD technique for different values of α, β, ξ. (b) Asymptotic average BER analysis under both HD and IM/DD technique for different values of α, β, ξ.

However, the AOA fluctuation of the UAV may cause a bottleneck in improving the system outage performance.

The outage performance under different threshold SNR using IM/DD technique is shown in Fig. 5. The turbulence level is assumed to moderate turbulence and the pointing errors are set as $\xi_1 = 2.1$, $\xi_2 = 2.7$. As can be seen, it can be inferred that the outage performance decreases with an increasing of threshold γ_{th}. For example, at SNR $= 30$, for our proposed scheme,$\gamma_{th} = 5$ dB yields an outage probability of 6.07×10^{-4} while $\gamma_{th} = 15$ dB yields an outage probability of 2.74×10^{-2}. Also, it's evident that our proposed scheme is superior to the FSO/FSO scheme and FSO/RF scheme under different threshold SNR, especially in the case $\gamma_{th} = 5$ dB. Moreover, the outage performance of FSO/RF scheme is better than FSO/FSO scheme which is because that the RF link is relatively not sensitive to different weather conditions. Furthermore, our proposed scheme can flexibly select different work modes to adapt to complex weather conditions, so owns the best outage performance.

In Fig. 6(a), we analyze the asymptotic outage performance under both HD and IM/DD technique for different values of α, β, ξ. We set two different sets of turbulence conditions and pointing error values to verify the correctness and tightness of our asymptotic analysis. It can clearly see that the curves have the same slopes for $(\alpha, \beta, \xi) = (1.36, 1.80, 2.1)$ and $(\alpha, \beta, \xi) = (3.62, 1.36, 2.7)$ with IM/DD technique or HD technique, which means they have the same diversity. The reason is that the diversity order of our proposed system is determined by the minimum value of parameters α, β, ξ, and this also verifies the correctness of our asymptotic analysis. In addition, the asymptotic analysis of average BER in Fig. 6(b) also showed similar results. Therefore, it can be inferred that the link outage performance and average BER performance are determined by the smallest value of turbulence parameters and pointing errors coefficients, which also provide some guidance when we consider compensating for the link performance.

Fig. 7 depicts the average bit-error rate with OOK modulation under different pointing errors using IM/DD technique. We can observe that the average BER performance gets better with a higher value of ξ, which due to the fact that a higher value of ξ means that optical receiver can receive more optical power, so

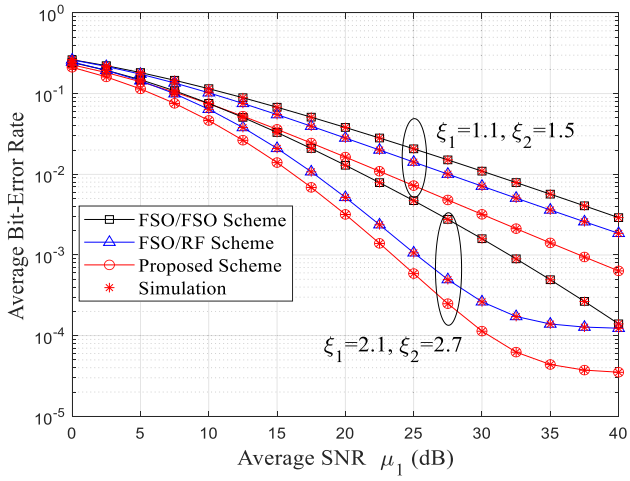

Fig. 7. Average bit-error rate with OOK modulation under different pointing errors using IM/DD technique.

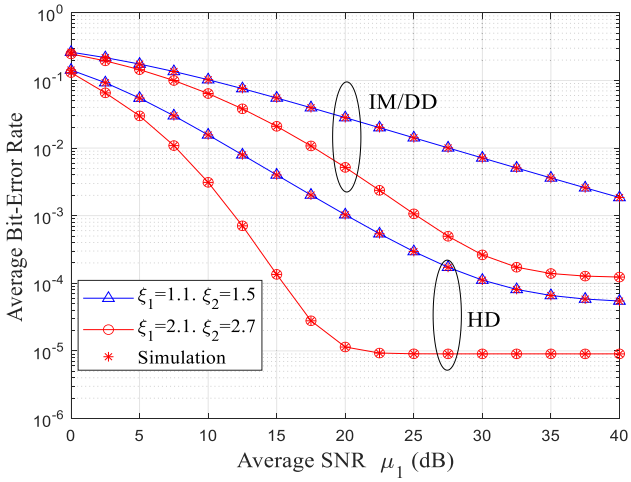

Fig. 8. Average bit-error rate using both IM/DD and HD technique under different pointing errors.

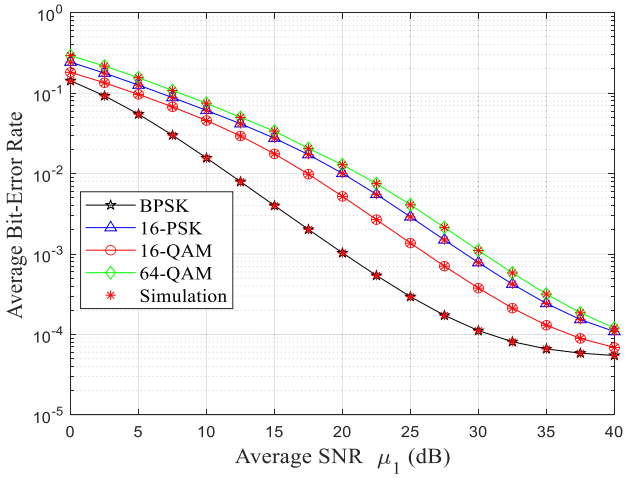

Fig. 9. Average bit-error rate for different modulation schemes using HD technique.

the performance of both satellite-to-HAPS FSO link and HAPS-to-GS FSO link will be further improved. Furthermore, it can be observed that our proposed scheme can achieve better average BER performance than both FSO/FSO scheme and FSO/RF scheme especially in higher value of ξ which is due to the fact that our proposed scheme can select the transmission mode which is most suitable for the current weather conditions. Similar to Fig. 4, the average BER tends to a saturation as μ_1 continues increasing, which can be attributed to maximum transmit power limitation of HAPS and effect of the AOA fluctuation.

The average bit-error rate using both IM/DD technique and HD technique under different pointing errors is depicted in Fig. 8. Clearly, we can observe that the average BER performance can be improved with a higher value of ξ. In addition, HD technique can achieve a considerable improvement of average BER compared to IM/DD technique in different pointing error parameters. For example, when $\xi_1 = 2.1$, $\xi_2 = 2.7$, in order to achieve average BER of 10^{-4}, the average SNR of IM/DD technique is 30 dB while the average SNR of HD technique is 15 dB. Moreover, the diversity order of HD technique is higher than IM/DD technique which is also consistent with our asymptotic analysis in Section IV. We can also observe that the average BER tends to a saturation as μ_1 continues increasing, and the reason is that with a high value of μ_1, the average BER of our proposed scheme is mainly determined by the average BER caused by the first term of formula (38). The maximum transmission power of HAPS also has a certain impact.

The average bit-error rate for BPSK, 16-PSK, 16-QAM and 64-QAM modulation schemes under HD detection technique is plotted in Fig. 9. We can observe that the 64-QAM owns the worst average BER performance as expected, and 16-QAM outperforms 16-PSK which is consistent with [50]. BPSK modulation can achieve the best average BER performance compared to the other modulation techniques. Thus, BPSK modulation under HD technique is a better choice for achieving stable and reliable transmission under complex weather conditions. Also, average BER tends to saturate as μ_1 continues increasing and the gap of average BER between different modulation methods gradually decrease. Furthermore, from Figs. 7 and 8, we can infer that HD technology using BPSK, 16-PSK, 16-QAM and 64-QAM modulation scheme performs much better than IM/DD technology using OOK modulation scheme.

The ergodic capacity using both IM/DD and HD technique under different pointing errors is shown in Fig. 10. The turbulence level is assumed to moderate turbulence and the average SNR of HAP-to-GS link is assumed as 20 dB. It can be seen that with the increasing of pointing error coefficient, the ergodic capacity performance is improved for different detection techniques. It is due to the fact that as the pointing error coefficient increases, the impact of pointing error reduces, and the capacity performance of both satellite-to-HAPS FSO link and HAPS-to-GS FSO link improves significantly. The HD technology outperforms IM/DD technology under different pointing error parameters, for example, at SNR = 30 dB, for $\xi_1 = 2.1$, $\xi_2 = 2.7$, the ergodic capacity improves by 28.2% using HD technology rather IM/DD technology. Therefore, HD detection can be a better choice for improving the capacity performance of satellite-to-GS backbone links under complex weather conditions. Finally, the analytical

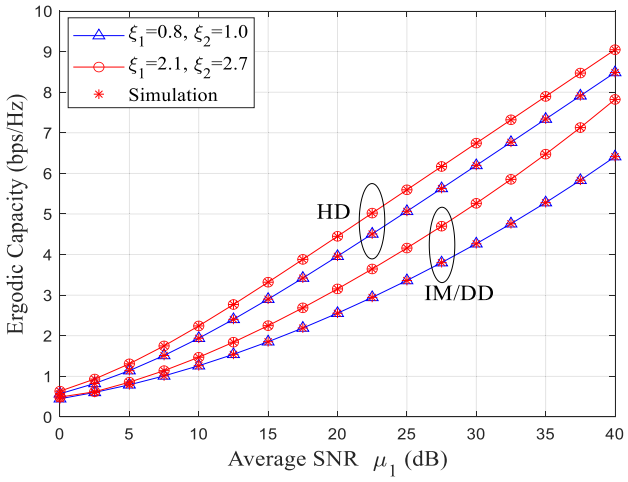

Fig. 10. Ergodic capacity using both IM/DD and HD technique under different pointing errors.

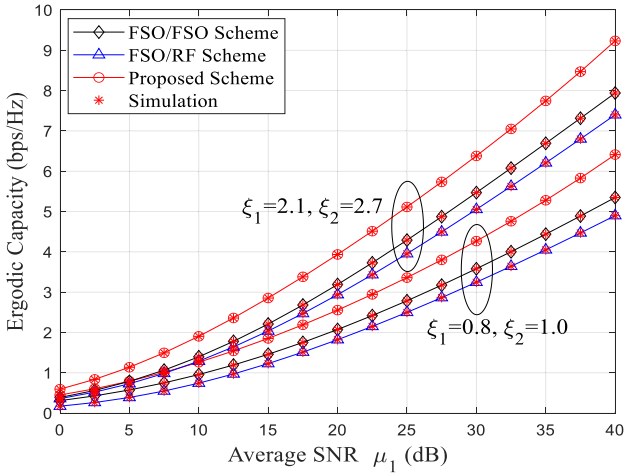

Fig. 11. Ergodic capacity for different schemes using IM/DD technique under different pointing errors.

results match well with the numerical simulation counterparts which can verify the correctness of our derivation.

Fig. 11 presents the ergodic capacity for different schemes using IM/DD technique under different pointing errors. It can be observed that as the pointing error deteriorates, the ergodic capacity performance of the system decreases which is due to the that the ergodic capacity of both satellite-to-HAPS FSO link and HAPS-to-GS FSO link will decrease with a smaller value of ξ. And our proposed scheme is superior compared to the FSO/FSO scheme and FSO/RF scheme under different pointing errors. It is because that our proposed scheme can select the transmission modes with better ergodic capacity performance. Interestingly, with the increasing of μ_1 and the pointing error coefficient, the superiority of our proposed scheme becomes more evident. In a nutshell, our proposed scheme can further leverage the capacity advantage of FSO links in satellite terrestrial integrated network and achieve high-speed transmission of satellite terrestrial backbone links.

VI. Conclusion

In this paper, we have proposed a new RIS-assisted UAV relay scheme for hybrid FSO/RF satellite terrestrial integrated network where the RF link is modeled by shadowed Rician distribution while the FSO link is assumed to follow the Gamma-Gamma distribution. The system performance is evaluated in terms of outage probability, average BER and ergodic capacity where the FSO link operates under either IM/DD or HD techniques. These performance metrics are obtained in the form of bivariate Fox's H function and bivariate Meijer's G function. Asymptotic results and diversity order are also obtained to get more insights. Numerical results reveal the notable effect of atmospheric turbulence, pointing errors, and threshold SNR on the overall system performance. Increasing the turbulence level can deteriorate the system performance and a higher pointing error parameter can significantly improve the system performance. The system performance can also be improved with a smaller threshold SNR. Furthermore, the HD technique can considerably improve the system outage probability, average BER and ergodic capacity compared to IM/DD technology. Moreover, our proposed scheme can outperform the FSO/FSO scheme and FSO/RF scheme due to the flexible weather dependent link switching and selection. Finally, the system outage probability and average BER tend to saturation due to the limitation of maximum transmission power of HAPS and the influence of AOA.

Appendix A
FSO Link Turbulence Parameters

This appendix gives the calculation method of turbulence parameters α and β of the FSO link. Considering the beam wander, the turbulence parameter α and β can be expressed as

$$\alpha = \left[5.95(H_s - h_p)^2 \sec^2(\varsigma) \left(\frac{2W_0}{r_0}\right)^{\frac{5}{3}} \left(\frac{\alpha_{pe}}{W}\right)^2 + \exp\left(\frac{0.49\sigma_{Bu}^2}{\left(1+0.56\sigma_{Bu}^{\frac{12}{5}}\right)^{\frac{7}{6}}}\right)\right] \tag{A.1}$$

$$\beta = \left[\exp\left(\frac{0.51\sigma_{Bu}^2}{\left(1+0.69\sigma_{Bu}^{\frac{12}{5}}\right)^{\frac{5}{6}}}\right) - 1\right]^{-1} \tag{A.2}$$

Where H_s is the altitude of the LEO satellite in m, h_p is the altitude of the HAP in m. ς is the zenith angle, W_0 refers to beam radius at the transmitter and W denotes beam radius at the receiver expressed as $W = W_0\sqrt{\Theta_0^2 + \Lambda_0^2}$, Θ and Λ_0 are the transmitter beam parameters. r_0 is the Fried parameter, α_{pe} denotes the beam wander-induced angular pointing error and σ_{Bu}^2 is the Rytov variance given by

$$\sigma_{Bu}^2 = 2.25k^{\frac{7}{6}}(H_s - h_p)^{\frac{5}{6}} \sec^{\frac{11}{6}}(\varsigma) \int_{h_p}^{H_s} C_n^2(h) \times \left(1 - \frac{h-h_p}{H_s - h_p}\right)^{\frac{5}{6}} \left(\frac{h-h_p}{H_s - h_p}\right)^{\frac{5}{6}} dh \tag{A.3}$$

The Fried parameter r_0 can be expressed as

$$r_0 = \left[0.42 \sec(\varsigma) k^2 \int_{h_p}^{H_s} C_n^2(h) dh\right]^{-\frac{3}{5}} \tag{A.4}$$

$C_n^2(h)$ is the refractive index structure parameter given as [18, eq. (52)]

$$C_n^2(h) = 0.00594\left(\frac{\omega}{27}\right)^2 \left(10^{-5}h\right)^{10} \exp\left(-\frac{h}{1000}\right) + 2.7\times 10^{-16} \exp\left(-\frac{h}{1500}\right) + C_n^2(0) \exp\left(-\frac{h}{100}\right) \tag{A.5}$$

Where $C_n^2(0)$ refers to the ground level turbulence in $m^{-2/3}$ and ω denotes the rms windspeed in m/s. α_{pe} can be expressed by $\alpha_{pe} = \sigma_{pe}/L$, where σ_{pe} is the beam wander-induced pointing error variance

$$\sigma_{pe}^2 = 0.54 (H_s - h_p) \sec^2(\varsigma) \left(\frac{\lambda}{2W_0}\right)^2 \left(\frac{2W_0}{r_0}\right)^{\frac{5}{3}} \times \left[1 - \left(\frac{C_r^2 W_0^2/r_0^2}{1 + C_r^2 W_0^2/r_0^2}\right)^{\frac{1}{6}}\right] \tag{A.6}$$

And L is the distance between transmitter and receiver express as $L = (H_s - h_p)\sec(\varsigma)$.

Appendix B
CDF of the End-to-End SNR of Mode 1

The CDF of end-to-end SNR of mode 1 under AF relay with a fixed gain Q can be written as

$$F_{\gamma_1}(\gamma) = \Pr\left[\frac{\gamma_{SH}^f \gamma_{HG}^f}{\gamma_{HG}^f + Q} < \gamma\right] \tag{B.1}$$

Which can be further expressed as

$$\begin{aligned} F_{\gamma_1}(\gamma) &= \int_0^\infty F_{\gamma_{SH}^f}\left(\frac{\gamma\left(\gamma_{HG}^f + Q\right)}{\gamma_{HG}^f}\right) f_{\gamma_{HG}^f}\left(\gamma_{HG}^f\right) d\gamma_{HG}^f \\ &= \int_{x=0}^\infty \int_{t=0}^\gamma f_{\gamma_{SH}^f}(t) f_{\gamma_{HG}^f}(x)\, dtdx \\ &\quad + \int_{x=0}^\infty \int_{t=\gamma}^{\gamma+\frac{Qr}{x}} f_{\gamma_{SH}^f}(t) f_{\gamma_{HG}^f}(x)\, dtdx \end{aligned} \tag{B.2}$$

Interchanging the integrals yields, the CDF becomes

$$\begin{aligned} F_{\gamma_1}(\gamma) &= \int_{t=0}^\gamma \int_{x=0}^\infty f_{\gamma_{SH}^f}(t) f_{\gamma_{HG}^f}(x)\, dxdt \\ &\quad + \int_{t=\gamma}^\infty \int_{x=0}^{\frac{Q\gamma}{t-\gamma}} f_{\gamma_{SH}^f}(t) f_{\gamma_{HG}^f}(x)\, dxdt \\ &= F_{\gamma_{SH}^f}(\gamma) + \int_\gamma^\infty F_{\gamma_{HG}^f}\left(\frac{Q\gamma}{t-\gamma}\right) f_{\gamma_{SH}^f}(t)\, dt \end{aligned} \tag{B.3}$$

Substituting (17), (18) and (19) into (B.3), we can obtain

$$\begin{aligned} F_{\gamma_1}(\gamma) = F_{\gamma_{SH}^f}(\gamma) + \int_{\gamma=0}^\infty \frac{1}{t} G_{b_2+1,3b_2+1}^{3b_2,1}\left[\frac{D_2^{b_2}}{b_2^{2b_2}\mu_2}\frac{Q\gamma}{t-\gamma}\middle| \begin{matrix}1, E_3\\ E_4, 0\end{matrix}\right] \\ \times G_{1,3}^{3,0}\left[\frac{\alpha_1\beta_1\xi_1^2}{\xi_1^2+1}\left(\frac{t}{\mu_1}\right)^{\frac{1}{b_1}}\middle| \begin{matrix}\xi_1^2+1\\ \xi_1^2, \alpha_1, \beta_1\end{matrix}\right] dt \end{aligned} \tag{B.4}$$

Changing the integrals variable $x = t - r$, and using definition of the Meijer's G function in [41, eq. (9.301)], then using the integral identity in [41, eq. (3.194/3)], (B.4) can be re-written as

$$\begin{aligned} F_{\gamma_1}(\gamma) = F_{\gamma_{SH}^f}(\gamma) - \frac{\xi_1^2 F^2}{b_1 \Gamma(\alpha_1)\Gamma(\beta_1)} \frac{1}{(2\pi i)^2} \\ \int_{L_1}\int_{L_2} \frac{\prod_{i=0}^{b_2-1}\Gamma\left(\frac{\xi_2^2+i}{b_2} - s\right)}{\prod_{i=0}^{b_2-1}\Gamma\left(\frac{\xi_2^2+1+i}{b_2} - s\right)} \\ \times \prod_{i=0}^{b_2-1}\Gamma\left(\frac{\alpha_2+i}{b_2} - s\right) \times \prod_{i=0}^{b_2-1}\Gamma\left(\frac{\beta_2+i}{b_2} - s\right) \\ \times \Gamma(-s) \times \Gamma\left(\frac{t}{b_1} + s\right) \\ \times \frac{\Gamma\left(\xi_1^2+t\right)\Gamma(\alpha_1+t) \times \Gamma(\beta_1+t)}{\Gamma(\xi_1^2+1+t)\Gamma\left(1+\frac{t}{b_1}\right)} \\ \left(\frac{D_2^{b_2} Q}{b_2^{2b_2}\mu_2}\right)^s \left(\frac{\xi_1^2+1}{\alpha_1\beta_1\xi_1^2}\left(\frac{\mu_1}{\gamma}\right)^{\frac{1}{b_1}}\right)^t ds dt \end{aligned} \tag{B.5}$$

Where L_1 and L_2 are the s-plane and t-plane contours, respectively. By using [47, eq. (1.1)], we can obtain the end-to-end SNR given in (30).

Appendix C
CDF of the End-to-End SNR of Mode 4

This appendix derives closed-form expression for the CDF of $F_4(\gamma)$. Similar to (B.1)–(B.3), we start by deriving the CDF of

$$\begin{aligned} F_{\gamma_4}(\gamma) &= \int_{t=0}^\gamma \int_{x=0}^\infty f_{\gamma_{SH}^f}(t) f_{\gamma_{HG}^f}(x)\, dxdt \\ &\quad + \int_{t=\gamma}^\infty \int_{x=0}^{\frac{C\gamma}{t-\gamma}} f_{\gamma_{SH}^f}(t) f_{\gamma_{HG}^f}(x)\, dxdt \\ &= F_{\gamma_{SH}^f}(\gamma) + \int_0^\infty F_{\gamma_{HG}^r}\left(\frac{C\gamma}{z}\right) f_{\gamma_{SH}^f}(z+\gamma)\, dz \end{aligned} \tag{C.1}$$

Substituting (17), (18) and (28) into (C.1), using the definition of the Meijer's G function given in [41, eq. (9.301)], transforming the exp (·) function to its correspondent Meijer's G function [42, eq. (01.03.26.0004.01)], and interchanging the integrals, the

CDF can be expressed as

$$F_{\gamma_4}(\gamma) = 1 - \frac{\xi_1^2}{b_1\Gamma(\alpha_1)\Gamma(\beta_1)}\left(\frac{2bm}{2bm+\Omega}\right)^{m-1} \times \sum_{k=0}^{m-1}\sum_{j=0}^{k}\frac{(-1)^k(1-m)_k}{k!j!} \times \left(\frac{\Omega}{2bm}\right)^k\left(\frac{Cm\gamma}{\bar{\gamma}_{HG}^r}\right)^j\frac{1}{(2\pi i)^2} \int_{L_1}\int_{L_2}\Gamma(-s)\left(\frac{Cm\gamma}{\bar{\gamma}_{HG}^r}\right)^s\frac{\Gamma(\xi_1^2-t)\Gamma(\alpha_1-t)}{\Gamma(\xi_1^2+1-t)} \times \Gamma(\beta_1-t)\times\left(\frac{\alpha_1\beta_1\xi_1^2}{(\xi_1^2+1)\mu_1^{\frac{1}{b_1}}}\right)^t \int_0^\infty y^{-j-s}(y+\gamma)^{\frac{t}{b_1}-1}dzdsdt \tag{C.2}$$

where L_1 and L_2 represent the s-plane and t-plane contours, respectively. Accord to [41, eq. (3.194/3)] and then [41, eq. (8.384/1)], $\int_0^\infty y^{-j-s}(y+\gamma)^{\frac{t}{b_1}-1}dy$ can reduce to $(\gamma)^{\frac{t}{b_1}-s-j}\Gamma(1-j-s)\Gamma(j+s-\frac{t}{b_1})/\Gamma(1-\frac{t}{b_1})$, and by using variable replacement, C.2 can be written as

$$F_{\gamma_4}(\gamma) = 1 - \frac{\xi_1^2}{\Gamma(\alpha_1)\Gamma(\beta_1)}\left(\frac{2bm}{2bm+\Omega}\right)^{m-1} \times \sum_{k=0}^{m-1}\sum_{j=0}^{k}\frac{(-1)^k(1-m)_k}{k!j!} \times \left(\frac{\Omega}{2bm}\right)^k\frac{1}{(2\pi i)^2}\int_{L_1}\int_{L_2}\Gamma(s+t) \Gamma(j-s)\Gamma(1-s)\left(\frac{Cm}{\bar{\gamma}_{HG}^r}\right)^s \times\frac{\Gamma(\xi_1^2+b_1t)\Gamma(\alpha_1+b_1t)\Gamma(\beta_1+b_1t)}{\Gamma(\xi_1^2+1+b_1t)\Gamma(1+t)} \times\left(\frac{(\xi_1^2+1)^{b_1}\mu_1}{\alpha_1\beta_1\xi_1^2\gamma}\right)^t dsdt \tag{C.3}$$

Plugging $\Gamma(nz) = n^{nz-\frac{1}{2}}(2\pi)^{\frac{1-n}{2}}\prod_{k=0}^{n-1}\Gamma(z+\frac{k}{n}), (\mathrm{n}\in\mathrm{N})$ in (C.3) yields

$$F_{\gamma_4}(\gamma) = 1 - \frac{\xi_1^2 b_1^{\alpha_1+\beta_1-2}}{\Gamma(\alpha)\Gamma(\beta)(2\pi)^{b_1-1}}\left(\frac{2bm}{2bm+\Omega}\right)^{m-1} \times \sum_{k=0}^{m-1}\sum_{j=0}^{k}\frac{(-1)^k(1-m)_k}{k!j!} \times \left(\frac{\Omega}{2bm}\right)^k\frac{1}{(2\pi i)^2}\int_{L_1}\int_{L_2}\Gamma(s+t)\Gamma(j-s) \Gamma(1-s)\left(\frac{Cm}{\bar{\gamma}_{HG}^r}\right)^s\frac{\prod_{i=0}^{b_1-1}\Gamma(\frac{\xi_1^2+i}{b_1}+t)}{\prod_{i=0}^{b_1-1}\Gamma\left(\frac{\xi_1^2+1+i}{b_1}+t\right)} \frac{\prod_{i=0}^{b_1-1}\Gamma(\frac{\alpha_1+i}{b_1}+t)\prod_{i=0}^{b_1-1}\Gamma(\frac{\beta_1+i}{b_1}+t)}{\Gamma(t+1)} \times\left(\frac{(\xi_1^2+1)^{b_1}b_1^{2b_1}\mu_1}{(\alpha_1\beta_1\xi_1^2)^{b_1}\gamma}\right)^t dsdt \tag{C.4}$$

With the help of [48, eq. (1)], the CDF of can be derived in terms of the bivariate Meijer's G function as

$$F_{\gamma_4}(\gamma) = 1 - \frac{\xi_1^2 b_1^{\alpha_1+\beta_1-2}}{\Gamma(\alpha)\Gamma(\beta)(2\pi)^{b_1-1}}\left(\frac{2bm}{2bm+\Omega}\right)^{m-1} \times \sum_{k=0}^{m-1}\sum_{j=0}^{k}\frac{(-1)^k(1-m)_k}{k!j!} \times \left(\frac{\Omega}{2bm}\right)^k \times G_{1,0:0,2:3b_1,b_1+1}^{1,0:2,0:0,3b_1}\left[0\left|-\atop j,1\right.\right|\Delta(b_1,-\xi_1^2),0\left|K_1\atop\Delta(b_1,-\xi_1^2),0\right.\left|\frac{Cm}{\bar{\gamma}_{HG}^r},\frac{b_1^{2b_1}(\xi_1^2+1)^{b_1}\mu_1}{(\alpha_1\beta_1\xi_1^2)^{b_1}\gamma}\right.\right] \tag{C.5}$$

Where $K_1 = \Delta(b_1, 1-\xi_1^2), \Delta(b_1, 1-\alpha_1), \Delta(b_1, 1-\beta_1)$, $\Delta(b_1,\mu) = \frac{\mu}{b_1}, \frac{\mu+1}{b_1}, \ldots, \frac{\mu+b_1-1}{b_1}$. The PDF can be obtained by taking the derivative of (C.5), given as

$$f_{\gamma_4}(\gamma) = \frac{\xi_1^2 b_1^{\alpha_1+\beta_1-2}}{\Gamma(\alpha)\Gamma(\beta)(2\pi)^{b_1-1}\gamma}\left(\frac{2bm}{2bm+\Omega}\right)^{m-1} \times \sum_{k=0}^{m-1}\sum_{j=0}^{k}\frac{(-1)^k(1-m)_k}{k!j!} \times \left(\frac{\Omega}{2bm}\right)^k \times G_{1,0:0,2:3b_1,b_1+1}^{1,0:2,0:0,3b_1}\left[0\left|-\atop j,1\right.\right|\Delta(b_1,-\xi_1^2),1\left|K_1\atop\Delta(b_1,-\xi_1^2),1\right.\left|\frac{Cm}{\bar{\gamma}_{HG}^r},\frac{b_1^{2b_1}(\xi_1^2+1)^{b_1}\mu_1}{(\alpha_1\beta_1\xi_1^2)^{b_1}\gamma}\right.\right] \tag{C.6}$$

Appendix D
Average Bit-Reeor Rate

Substituting (B.5) into (35) and using [41, eq (3.381/4)], the average BER can be re-written as (D1) shown at the bottom of the next page.

Where F_p is given by

$$F_p = F^1\sum_{u=1}^{n}G_{b_1+2,3b_1+1}^{3b_1,2}\left(\frac{D_1^{b_1}}{b_1^{2b_1}\mu_1 q_u}\left|\begin{matrix}11-pE_1\\E_20\end{matrix}\right.\right) \tag{D.2}$$

Using [47, eq. (1.1)], (D.1), can be written in the form of bivariate Fox's H function given in (36)

Appendix E
Ergodic Capacity

The PDF of end-to-end SNR of mode 1 can be obtained by differentiating (30), and using [41, eq. (8.331/1)] given as (E1) shown at the bottom of the next page.

$$P_{e,1}=\frac{\sigma}{2\Gamma(p)}F_p-\frac{\sigma\xi_1^2F^2}{2b_1\Gamma(\alpha_1)\Gamma(\beta_1)\Gamma(p)}\frac{1}{(2\pi i)^2}\sum_{u=1}^{n}\int_{L_1}\int_{L_2}\Gamma\left(\frac{t}{b_1}+s\right)\times\frac{\prod_{i=0}^{b_2-1}\Gamma\left(\frac{\xi_2^2+i}{b_2}-s\right)\prod_{i=0}^{b_2-1}\Gamma\left(\frac{\alpha_2+i}{b_2}-s\right)\prod_{i=0}^{b_2-1}\Gamma\left(\frac{\beta_2+i}{b_2}-s\right)\times\Gamma(-s)}{\prod_{i=0}^{b_2-1}\Gamma\left(\frac{\xi_2^2+1+i}{b_2}-s\right)}\frac{\Gamma\left(\xi_1^2+t\right)\Gamma(\alpha_1+t)\Gamma(\beta_1+t)\Gamma\left(p-\frac{t}{b_1}\right)}{\Gamma(\xi_1^2+1+t)\Gamma\left(1+\frac{t}{b_1}\right)}\times\left(\frac{D_2^{b_2}Q}{b_2^{2b_2}\mu_2}\right)^s\left(\frac{\xi_1^2+1}{\alpha_1\beta_1\xi_1^2}(\mu_1q_u)^{\frac{1}{b_1}}\right)^t dsdt \tag{D.1}$$

$$f_1(\gamma)=f_{\gamma_{SH}^f}(\gamma)+\frac{\xi_1^2F^2}{b_1\Gamma(\alpha_1)\Gamma(\beta_1)\gamma}\frac{1}{(2\pi i)^2}\int_{L_1}\int_{L_2}\Gamma\left(\frac{t}{b_1}+s\right)\times\frac{\prod_{i=0}^{b_2-1}\Gamma\left(\frac{\xi_2^2+i}{b_2}-s\right)\prod_{i=0}^{b_2-1}\Gamma\left(\frac{\alpha_2+i}{b_2}-s\right)\prod_{i=0}^{b_2-1}\Gamma\left(\frac{\beta_2+i}{b_2}-s\right)\Gamma(-s)}{\prod_{i=0}^{b_2-1}\Gamma\left(\frac{\xi_2^2+1+i}{b_2}-s\right)}\times\frac{\Gamma\left(\xi_1^2+t\right)\Gamma(\alpha_1+t)\Gamma(\beta_1+t)}{\Gamma(\xi_1^2+1+t)\Gamma\left(\frac{t}{b_1}\right)}\times\left(\frac{D_2^{b_2}Q}{b_2^{2b_2}\mu_2}\right)^s\left(\frac{\xi_1^2+1}{\alpha_1\beta_1\xi_1^2}\left(\frac{\mu_1}{\gamma}\right)^{\frac{1}{b_1}}\right)^t dsdt \tag{E.1}$$

Substituting (E.1), into (40), and using [42, eq. (07.34.03.0456.01)], $\overline{C}_{EC,1}$ can be written as

$$\overline{C}_{EC,1}=F_s+\frac{\xi_1^2F^2}{b_1\Gamma(\alpha_1)\Gamma(\beta_1)}\frac{1}{(2\pi i)^2}\int_{L_1}\int_{L_2}\Gamma\left(\frac{t}{b_1}+s\right)\times\prod_{i=0}^{b_2-1}\Gamma\left(\frac{\xi_2^2+i}{b_2}-s\right)\times\frac{\prod_{i=0}^{b_2-1}\Gamma\left(\frac{\alpha_2+i}{b_2}-s\right)\prod_{i=0}^{b_2-1}\Gamma\left(\frac{\beta_2+i}{b_2}-s\right)\Gamma(-s)}{\prod_{i=0}^{b_2-1}\Gamma\left(\frac{\xi_2^2+1+i}{b_2}-s\right)}\times\Gamma\left(\xi_1^2+t\right)\Gamma(\alpha_1+t)\times\frac{\Gamma(\beta_1+t)}{}\Gamma\left(\xi_1^2+1+t\right)\Gamma\left(\frac{t}{b_1}\right)\times\left(\frac{D_2^{b_2}Q}{b_2^{2b_2}\mu_2}\right)^s\left(\frac{\xi_1^2+1}{\alpha_1\beta_1\xi_1^2}\mu_1^{\frac{1}{b_1}}\right)^t\int_0^\infty\gamma^{-\frac{t}{b_1}-1}G_{2,2}^{1,2}\left[c\gamma\middle|\begin{matrix}1,1\\1,0\end{matrix}\right]d\gamma dsdt \tag{E.2}$$

Where F_s is obtained by using [42, eq. (07.34.21.0013.01)] given as

$$F_s=\frac{\xi_1^2b_1^{\alpha_1+\beta_1-2}}{(2\pi)^{b_1-1}\Gamma(\alpha_1)\Gamma(\beta_1)}G_{b_1+2,3b_1+2}^{3b_1+2,1}\left[\frac{D_1^{b_1}}{cb_1^{2b_1}\mu_1}\middle|\begin{matrix}0,1,E_1\\E_2,0,0\end{matrix}\right] \tag{E.3}$$

Using [42, eq. (07.34.21.0009.01)] and then [41, 8.331/1], (E.2) can be simplified as

$$\overline{C}_{EC,1}=F_s+\frac{\xi_1^2F^2}{b_1\Gamma(\alpha_1)\Gamma(\beta_1)}\frac{1}{(2\pi i)^2}\int_{L_1}\int_{L_2}\Gamma\left(\frac{t}{b_1}+s\right)\prod_{i=0}^{b_2-1}\Gamma\left(\frac{\xi_2^2+i}{b_2}-s\right)\times\frac{\prod_{i=0}^{b_2-1}\Gamma\left(\frac{\alpha_2+i}{b_2}-s\right)\prod_{i=0}^{b_2-1}\Gamma\left(\frac{\beta_2+i}{b_2}-s\right)\Gamma(-s)}{\prod_{i=0}^{b_2-1}\Gamma\left(\frac{\xi_2^2+1+i}{b_2}-s\right)}\Gamma\left(1-\frac{t}{b_1}\right)\Gamma\left(\xi_1^2+t\right)\times\frac{\Gamma(\alpha_1+t)\Gamma(\beta_1+t)\Gamma\left(\frac{t}{b_1}\right)}{\Gamma(\xi_1^2+1+t)\Gamma\left(1+\frac{t}{b_1}\right)}\times\left(\frac{D_2^{b_2}Q}{b_2^{2b_2}\mu_2}\right)^s\left(\frac{\xi_1^2+1}{\alpha_1\beta_1\xi_1^2}(c\mu_1)^{\frac{1}{b_1}}\right)^t dsdt \tag{E.4}$$

Now, using [47, eq. (1.1)], $\overline{C}_{EC,1}$ can be obtained in closed-form shown in (41).

REFERENCES

[1] E. Yaacoub and M.-S. Alouini, "A key 6G challenge and opportunity-connecting the base of the pyramid: A survey on rural connectivity," *Proc. IEEE*, vol. 108, no. 4, pp. 533–582, Apr. 2020.

[2] E. Lee, J. Park, D. Han, and G. Yoon, "Performance analysis of the asymmetric dual-hop relay transmission with mixed RF/FSO links," *IEEE Photon. Technol. Lett.*, vol. 23, no. 21, pp. 1642–1644, Nov. 2011.

[3] H. Kong, M. Lin, Z. Wang, J. Ouyang, and J. Cheng, "Ergodic capacity of high throughput satellite systems with mixed FSO-RF transmission," *IEEE Wireless Commun. Lett.*, vol. 10, no. 8, pp. 1732–1736, Aug. 2021.

[4] P. K. Singya and M.-S. Alouini, "Performance of UAV-assisted multiuser terrestrial-satellite communication system over mixed FSO/RF channels," *IEEE Trans. Aerosp. Electron. Syst.*, vol. 58, no. 2, pp. 781–796, Apr. 2022.

[5] R. Samy, H.-C. Yang, T. Rakia, and M.-S. Alouini, "Ergodic capacity analysis of satellite communication systems with SAG-FSO/SH-FSO/RF transmission," *IEEE Photon. J.*, vol. 14, no. 5, Oct. 2022, Art. no. 7347909.

[6] A. Majumdar, Z. Ghassemlooy, and A. Raj, *Principles and Applications of Free Space Optical (FSO) Communication*. London, U.K.: IET, 2019.

[7] S. Song, J. Wu, Y. Liu, and L. Guo, "A novel low-complexity high-order DPSK system with constellation reconstruction for FSO communication," *IEEE Wireless Commun. Lett.*, vol. 11, no. 10, pp. 2031–2035, Oct. 2022.

[8] V. Sandeep, D. S. Gurjar, S. Yadav, P. Pattanayak, and Y. Jiang, "On the performance analysis of V2N mixed RF and hybrid FSO/RF communication system," *IEEE Photon. J.*, vol. 14, no. 6, Dec. 2022, Art. no. 7361114.

[9] H. D. Le and A. T. Pham, "On the design of FSO-based satellite systems using incremental redundancy hybrid ARQ protocols with rate adaptation," *IEEE Trans. Veh. Technol.*, vol. 71, no. 1, pp. 463–477, Jan. 2022.

[10] C. Zhai, "Performance of rectangular QAM/FSO communication systems in the anisotropic non-Kolmogorov ground-to-satellite uplink," *J. Opt. Commun. Netw.*, vol. 14, no. 9, pp. 713–724, Sep. 2022.

[11] B. Bag, A. Das, C. Bose, and A. Chandra, "Improving the performance of a DF relay-aided FSO system with an additional source–relay mmWave RF backup," *J. Opt. Commun. Netw.*, vol. 12, no. 12, pp. 390–402, Dec. 2020.

[12] J. Perez, Z. Ghassemlooy, S. Rajbhandari, M. Ijaz, and H. L. Minh, "Ethernet FSO communications link performance study under a controlled fog environment," *IEEE Commun. Lett.*, vol. 16, no. 3, pp. 408–410, Mar. 2012.

[13] E. S. Altubaishi and K. Alhamawi, "Capacity analysis of hybrid AF multi-hop FSO/RF system under pointing errors and weather effects," *IEEE Photon. Technol. Lett.*, vol. 31, no. 15, pp. 1304–1307, Aug. 2019.

[14] P. Paul, M. R. Bhatnagar, and A. Jaiswal, "Alleviation of jamming in free space optical communication over Gamma-Gamma channel with pointing errors," *IEEE Photon. J.*, vol. 11, no. 5, Oct. 2019, Art. no. 7906418.

[15] S. Sharma, A. S. Madhukumar, and R. Swaminathan, "Switching-based cooperative decode-and-forward relaying for hybrid FSO/RF networks," *J. Opt. Commun. Netw.*, vol. 11, no. 6, pp. 267–281, Jun. 2019.

[16] M. Najafi, V. Jamali, and R. Schober, "Optimal relay selection for the parallel hybrid RF/FSO relay channel: Non-buffer-aided and buffer-aided designs," *IEEE Trans. Commun.*, vol. 65, no. 7, pp. 2794–2810, Jul. 2017.

[17] O. B. Yahia, E. Erdogan, and G. K. Kurt, "HAPS-assisted hybrid RF-FSO multicast communications: Error and outage analysis," *IEEE Trans. Aerosp. Electron. Syst.*, vol. 59, no. 1, pp. 140–152, Feb. 2023.

[18] S. R. S. Sharma, N. Vishwakarma, and A. S. Madhukumar, "HAPS-based relaying for integrated space-air-ground networks with hybrid FSO/RF communication: A performance analysis," *IEEE Trans. Aerosp. Electron. Syst.*, vol. 57, no. 3, pp. 1581–1599, Jun. 2021.

[19] S. K. Singh, K. Agrawal, K. Singh, C.-P. Li, and Z. Ding, "NOMA enhanced hybrid RIS-UAV-assisted full-duplex communication system with imperfect SIC and CSI," *IEEE Trans. Commun.*, vol. 70, no. 11, pp. 7609–7627, Nov. 2022.

[20] K. Guo and K. An, "On the performance of RIS-assisted integrated satellite-UAV-terrestrial networks with hardware impairments and interference," *IEEE Wireless Commun. Lett.*, vol. 11, no. 1, pp. 131–135, Jan. 2022.

[21] D. R. Pattanayak, V. K. Dwivedi, V. Karwal, A. Upadhya, H. Lei, and G. Singh, "Secure transmission for energy efficient parallel mixed FSO/RF system in presence of independent eavesdroppers," *IEEE Photon. J.*, vol. 14, no. 1, Feb. 2022, Art. no. 7307714.

[22] R. J. Li, T. Chen, L. H. Fan, and A. Dang, "Performance analysis of a multiuser dual-hop amplify-and-forward relay system with FSO/RF links," *J. Opt. Commun. Netw.*, vol. 11, no. 7, pp. 362–370, Jul. 2019.

[23] E. Zedini, A. Kammoun, and M.-S. Alouini, "Performance of multi-beam very high throughput satellite systems based on FSO feeder links with HPA nonlinearity," *IEEE Trans. Wireless Commun.*, vol. 19, no. 9, pp. 5908–5923, Sep. 2020.

[24] I. Ahmad, K. D. Nguyen, N. Letzepis, and G. Lechner, "On the next-generation high throughput satellite systems with optical feeder links," *IEEE Syst. J.*, vol. 15, no. 2, pp. 2000–2011, Jun. 2021.

[25] G. Xu, Z. Zheng, and W. Wang, "Dual-hop deep space-terrestrial FSO/RF communication under solar scintillation: Performance analysis and challenges," *China Commun.*, vol. 17, no. 7, pp. 27–37, Jul. 2020.

[26] G. Xu and Q. Zhang, "Mixed RF/FSO deep space communication system under solar scintillation effect," *IEEE Trans. Aerosp. Electron. Syst.*, vol. 57, no. 5, pp. 3237–3251, Oct. 2021.

[27] M. T. Dabiri, S. M. S. Sadough, and M. A. Khalighi, "Channel modeling and parameter optimization for hovering UAV-based free-space optical links," *IEEE J. Sel. Areas Commun.*, vol. 36, no. 9, pp. 2104–2113, Sep. 2018.

[28] J.-Y. Wang, Y. Ma, R.-R. Lu, J.-B. Wang, M. Lin, and J. Cheng, "Hovering UAV-based FSO communications: Channel modelling, performance analysis, and parameter optimization," *IEEE J. Sel. Areas Commun.*, vol. 39, no. 10, pp. 2946–2959, Oct. 2021.

[29] H. Kong, M. Lin, W.-P. Zhu, H. Amindavar, and M.-S. Alouini, "Multiuser scheduling for asymmetric FSO/RF links in satellite-UAV-terrestrial networks," *IEEE Wireless Commun. Lett.*, vol. 9, no. 8, pp. 1235–1239, Aug. 2020.

[30] X. Liu, C. Gu, K. Guo, M. Cheng, M. Lin, and W.-P. Zhu, "Robust beamforming and outage performance of uplink multiuser satellite-aerial-terrestrial networks with mixed RF-FSO channels," *IEEE Photon. J.*, vol. 13, no. 4, Aug. 2021, Art. no. 7300408.

[31] T. V. Nguyen, H. D. Le, N. T. Dang, and A. T. Pham, "On the design of rate adaptation for relay-assisted satellite hybrid FSO/RF systems," *IEEE Photon. J.*, vol. 14, no. 1, Feb. 2022, Art. no. 7304211.

[32] Y. Liang, G. Wang, and I. S. Ansari, "Mixed dual-hop FSO-RF communication systems through reconfigurable intelligent surface," *IEEE Commun. Lett.*, vol. 24, no. 7, pp. 1558–1562, Jul. 2020.

[33] S. Malik, P. Saxena, and Y. H. Chung, "Performance analysis of a UAV-based IRS-assisted hybrid RF/FSO link with pointing and phase shift errors," *J. Opt. Commun. Netw.*, vol. 14, no. 4, pp. 303–315, Apr. 2022.

[34] T. V. Nguyen, H. D. Le, and A. T. Pham, "On the design of RIS-UAV relay-assisted hybrid FSO/RF satellite-aerial-ground integrated network," *IEEE Trans. Aerosp. Electron. Syst.*, vol. 59, no. 6, pp. 757–771, Apr. 2023.

[35] O. B. Yahia, E. Erdogan, G. K. Kurt, I. Altunbas, and H. Yanikomeroglu, "A weather-dependent hybrid RF/FSO satellite communication for improved power efficiency," *IEEE Wireless Commun. Lett.*, vol. 11, no. 3, pp. 573–577, Mar. 2022.

[36] X. Li, Y. J. Li, S. H. Zhao, H. L. Tang, and L. Shao, "Performance analysis of weather-dependent satellite-terrestrial network with rate adaptation hybrid free-space optical and radio frequency link," *Int. J. Satell. Commun. Netw.*, vol. 41, no. 4, pp. 357–373, Jul. 2022.

[37] H. Kaushal and G. Kaddoum, "Optical communication in space: Challenges and mitigation techniques," *IEEE Commun. Surveys Tut.*, vol. 19, no. 1, pp. 57–96, Firstquarter 2017.

[38] S. Sharma, A. S. Madhukumar, and R. Swaminathan, "Performance of dual-hop hybrid FSO/RF system with pointing errors optimization," in *Proc. IEEE 91st Veh. Technol. Conf.*, 2020, pp. 1–5.

[39] A. A. Farid and S. Hranilovic, "Outage capacity optimization for free-space optical links with pointing errors," *J. Lightw. Technol.*, vol. 25, no. 7, pp. 1702–1710, Jul. 2007.

[40] L. C. Andrews and R. L. Phillips, *Laser Beam Propagation Through Random Media*. Bellingham, WA, USA: SPIE, 2005.

[41] I. S. Gradshteyn and I. M. Ryzhik, *Table of Integrals, Series and Products*. New York, NY, USA: Academic, 2000.

[42] Wolfram, "The Wolfram functions site," 2014. [Online]. Available: http://functions.wolfram.com

[43] I. S. Ansari, F. Yilmaz, and M.-S. Alouini, "Performance analysis of FSO links over unified Gamma-Gamma-turbulence channels," in *Proc. IEEE Veh. Technol. Conf.*, 2015 pp. 1–5.

[44] A. Abdi, W. C. Lau, M.-S. Alouini, and M.-S. Kaveh, "A new simple model for land mobile satellite channels: First- and second-order statistics," *IEEE Trans. Wireless Commun.*, vol. 2, no. 3, pp. 519–528, May 2003.

[45] J. F. Paris, "Closed-form expressions for Rician shadowed cumulative distribution function," *Electron. Lett.*, vol. 46, no. 13, pp. 952–953, Jun. 2010.

[46] A. Kilbas and M. Saigo, *H-Transforms: Theory and Applications*. Boca Raton, FL, USA: CRC Press, 2004.

[47] P. Mittal and K. Gupta, "An integral involving generalized function of two variables," *Proc. Indian Acad. Sci.–Sect. A*, vol. 75, pp. 117–123, 1972.

[48] S. Gupta, "Integrals involving products of G-functions," *Proc. Nat. Acad. Sci. India*, 1969, pp. 193–200.

[49] H. Kazemi, M. Uysal, and F. Touati, "Outage analysis of hybrid FSO/RF systems based on finite-state Markov chain modeling," in *Proc. 3rd Int. Workshop Opt. Wireless Commun.*, 2014, pp. 11–15.

[50] J. Proakis and M. Salehi, *Digital Communications* (Series McGraw-Hill International Edition). New York, NY, USA: McGraw-Hill, 2008.